

**Syntheses, Characterization, Functional Properties, and Structure-Property
Relationships of New Mixed Metal Oxides**

A Thesis

Presented to

the Faculty of the Department of Chemistry

University of Houston

In Partial Fulfillment

of the Requirement for the Degree

Master of Science

By

Hana Lee

May 2013

Syntheses, Characterization, Functional Properties, and Structure-Property

Relationships of New Mixed Metal Oxides

Hana Lee

APPROVED by:

Dr. P. Shiv Halasyamani, Chairman

Dr. Arnold M. Guloy

Dr. Angela Moeller

Dr. Shoujun Xu

Dr. James K. Meen

Dean, College of Natural Sciences and Mathematics

Acknowledgments

I would like to gratefully and sincerely thank Dr. P. Shiv Halasyamani for his outstanding support and for being an abundant source of motivation. I also want to take this opportunity to thank the other members of my graduate committee, Dr. Arnold M. Guloy, Dr. Angela Moeller, Dr. Shoujun Xu, and Dr. James K. Meen for their time reviewing my work and for contributing insightful comments.

I was fortunate to work with many members of the Dr. Halasyamani group at the University of Houston. I am pleased to thank Dr. Weiguo Zang, Dr. Elise Pachoud, Sunwoo Kim, and Thanh Thao Tran for their support and friendship. I am gratefully thankful to Dr. Jeongho Yeon, as a former group member. When I was desperate with research, he helped and mentored me to overcome my obstacles.

I want to thank my friends, Hyemee, Mijung, Bomee, Soojeong, Minyoung, Donghyun, Joonhee, and Chulsoon. Their friendship and cheerful spirit has always been a great source of encouragement to overcome everyday technical and non-technical challenges during my graduate life.

Finally yet importantly, I would like to thank my parents, my brother Hyunhee and my aunt Yeorang for their abundant encouragement, patience, and love. My achievements would not be possible without their ample help and inspiration. I owe every step of this journey to them.

Thank you, God.

**Syntheses, Characterization, Functional Properties, and Structure-Property
Relationships of New Mixed Metal Oxides**

An Abstract of a Thesis

Presented to

the Faculty of the Department of Chemistry

University of Houston

In Partial Fulfillment

of the Requirement for the Degree

Master of Science

By

Hana Lee

Abstract

Non-centrosymmetric (NCS) oxide materials are of significant interest because of their functional properties, for example, second-harmonic generating (SHG), piezoelectricity, ferroelectricity, and pyroelectricity. A number of design strategies have been discussed for creating NCS oxide materials. We have focused on using cations susceptible to second-order Jahn-Teller (SOJT) distortion. The distortion can occur in two different types of cations, d^0 transition metals (Ti^{4+} , V^{5+} , Nb^{5+} , Mo^{6+} , etc.) and cations with stereoactive lone-pair (Se^{4+} , Te^{4+} , I^{5+} , Tl^+ , Pb^{2+} , etc.), and results in asymmetric coordination environments. In this dissertation, we report on the syntheses, crystal structures, characterization, functional properties, and their crystal structure-physical property relationships.

Table of Contents

Acknowledgment	iii
Abstract	v
Table of Contents	vi
List of Figures	viii
List of Tables	x

CHAPTER 1. Background

1.1 Asymmetric coordination environments	1
1.2 Hexagonal tungsten oxide (HTO)	2
1.3 References	5

CHAPTER 2. Syntheses, Characterization, Functional Properties, and Structure-Property Relationships in Two New Oxides: $\text{Tl}_2\text{Cu}_2\text{Te}_7\text{O}_{17}$ and $\text{Tl}_2\text{Cu}_2\text{Te}_7\text{O}_{18}$

2.1 Abstract	7
2.2 Introduction	7
2.3 Experimental section	9
2.3.1 Synthesis	9
2.3.2 Characterization	10
2.4 Results and discussion	12

2.5 Conclusion	28
2.6 References	29

CHAPTER 3. Syntheses and Crystal Structure of New Polar Potassium Tungsten

Selenite: $K_2(WO_3)_3(SeO_3)$

3.1 Abstract	40
3.2 Introduction	40
3.3 Experimental section	41
3.3.1 Synthesis	41
3.3.2 Characterization	42
3.4 Results and discussion	43
3.5 Conclusion	46
3.6 References	51

List of Figures

Figure 1.1	Examples of (a) C_2 (b) C_3 , and (c) C_4 distortion for d^0 transition metals.	1
Figure 1.2	ORTEP (50% probability level ellipsoids) diagrams for asymmetric coordination environments of the lone-pair cations.	2
Figure 1.3	Ball-and-stick diagram of (a) $Rb(VO_2)_3(SeO_3)_2$ -HTO class 1, (b) $Rb_2(MoO_3)_3(SeO_3)$ – HTO class 2, and polyhedral diagram of (c) hexagonal tungsten oxide (HTO) topology.	3
Figure 2.1	Ball-and-stick and polyhedral diagram of $Tl_2Cu_2Te_7O_{17}$ in the <i>ac</i> -plane consisting of the TeO_3 , TeO_4 , and TeO_5 polyhedra (a) with and (b) without CuO_4 , CuO_5 polyhedra and Tl^+ cations.	15
Figure 2.2	Ball-and-stick and polyhedral diagram of $Tl_2Cu_2Te_7O_{18}$ in the <i>ab</i> -plane consisting of the TeO_3 , TeO_4 , and TeO_6 polyhedra (a) with and (b) without CuO_4 polyhedra and Tl^+ cations.	16
Figure 2.3	ORTEP (50% probability level ellipsoids) diagrams for (a) $Tl_2Cu_2Te_7O_{17}$ and (b) $Tl_2Cu_2Te_7O_{18}$.	17
Figure 2.4	Calculated and observed powder X-ray diffraction pattern for $Tl_2Cu_2Te_7O_{17}$ and $Tl_2Cu_2Te_7O_{18}$.	18
Figure 2.5	IR data and assignments for $Tl_2Cu_2Te_7O_{17}$ and $Tl_2Cu_2Te_7O_{18}$.	20
Figure 2.6	UV-vis diffuse reflectance spectroscopy data for $Tl_2Cu_2Te_7O_{17}$ and $Tl_2Cu_2Te_7O_{18}$.	22
Figure 2.7	Thermogravimetric analysis (TGA) and differential thermal analysis (DTA) diagrams for $Tl_2Cu_2Te_7O_{17}$ and $Tl_2Cu_2Te_7O_{18}$.	24
Figure 2.8	Powder X-ray diffraction data of residues for $Tl_2Cu_2Te_7O_{17}$ and $Tl_2Cu_2Te_7O_{18}$.	25
Figure 2.9	Powder second-harmonic generation for $Tl_2Cu_2Te_7O_{17}$.	27
Figure 2.10	Displacement vs. electric field loops for $Tl_2Cu_2Te_7O_{17}$.	27
Figure 3.1	Ball-and-stick (a) polyhedral (b) diagram of $K_2(WO_3)_3(SeO_3)$ in	

the *bc*-plane. 44

Figure 3.2 ORTEP (50% probability level ellipsoids) diagrams for the WO_6 and SeO_3 polyhedra in $\text{K}_2(\text{WO}_3)_3(\text{SeO}_3)$. The arrows represent the approximate directions of the distortion and polarization. 45

List of Tables

Table 2.1	Crystallographic data for $\text{Tl}_2\text{Cu}_2\text{Te}_7\text{O}_{17}$ and $\text{Tl}_2\text{Cu}_2\text{Te}_7\text{O}_{18}$.	32
Table 2.2	Atomic coordinates and equivalent isotropic displacement parameters (\AA^2) for $\text{Tl}_2\text{Cu}_2\text{Te}_7\text{O}_{17}$.	33
Table 2.3	Atomic coordinates and equivalent isotropic displacement parameters (\AA^2) for $\text{Tl}_2\text{Cu}_2\text{Te}_7\text{O}_{18}$.	34
Table 2.4	Selected bond distances (\AA) for $\text{Tl}_2\text{Cu}_2\text{Te}_7\text{O}_{17}$.	36
Table 2.5	Selected bond distances (\AA) for $\text{Tl}_2\text{Cu}_2\text{Te}_7\text{O}_{18}$.	37
Table 2.6	Detailed bond valence analysis $\text{Tl}_2\text{Cu}_2\text{Te}_7\text{O}_{17}$.	38
Table 2.7	Detailed bond valence analysis $\text{Tl}_2\text{Cu}_2\text{Te}_7\text{O}_{18}$.	39
Table 3.1	Crystallographic data for $\text{K}_2(\text{WO}_3)_3(\text{SeO}_3)$.	47
Table 3.2	Atomic coordinates and equivalent isotropic displacement parameters (\AA^2) for $\text{K}_2(\text{WO}_3)_3(\text{SeO}_3)$.	48
Table 3.3	Selected bond distances (\AA) for $\text{K}_2(\text{WO}_3)_3(\text{SeO}_3)$.	49
Table 3.4	Detailed bond valence analysis $\text{K}_2(\text{WO}_3)_3(\text{SeO}_3)$.	50

CHAPTER 1. Background

1.1 Asymmetric coordination environments

Our specific goal is to create new noncentrosymmetric (NCS) oxides with d^0 transition metals (Ti^{4+} , V^{5+} , Nb^{5+} , W^{6+} , Mo^{6+} , etc.) and lone-pair cations (Se^{4+} , Te^{4+} , I^{5+} , Tl^+ , Sn^{2+} , etc.). Both cations are in asymmetric environments susceptible to second-order Jahn-Teller (SOJT) distortions.¹⁻⁶ The nature of the structural changes exhibited by the two cations is quite different even though both cations are found in asymmetric coordination environments. The d^0 -transition metals-centered octahedra can be distorted toward either an edge (C_2 distortion), a face (C_3 distortion), or a corner (C_4 distortion).⁷ These distortions result in bond asymmetries that can be explained as a MO_6 octahedron: C_2 type distortion - two short, two long, and two normal M-O bonds; C_3 type distortion - three short, two long, and one normal M-O bonds; C_4 type distortion - one short, one long, and four normal M-O bonds (see Figure 1.1).

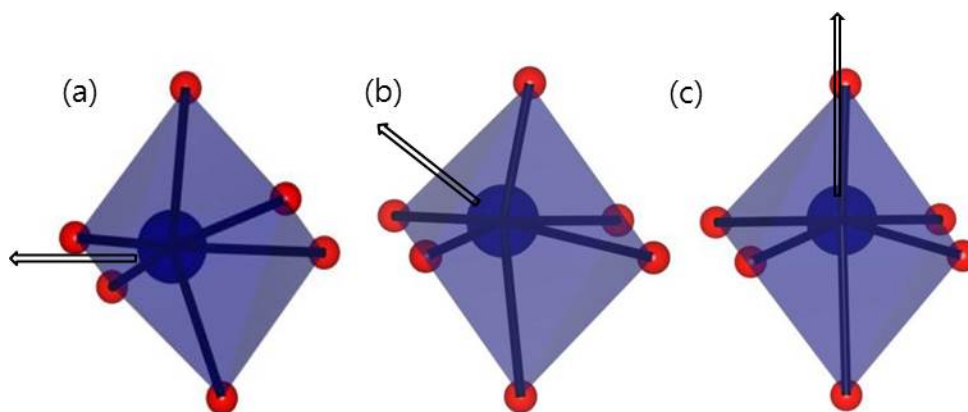


Figure 1.1 Examples of (a) C_2 (b) C_3 , and (c) C_4 distortion for d^0 transition metals.^{16,24,26}

The lone pair cations observed in asymmetric coordination environments are attributable to the lone-pair pushing the oxide ligands toward one side of the cation (see Figure 1.2).⁹ Thus, understanding their asymmetric coordination environments plays a crucial role in synthesizing new polar materials.

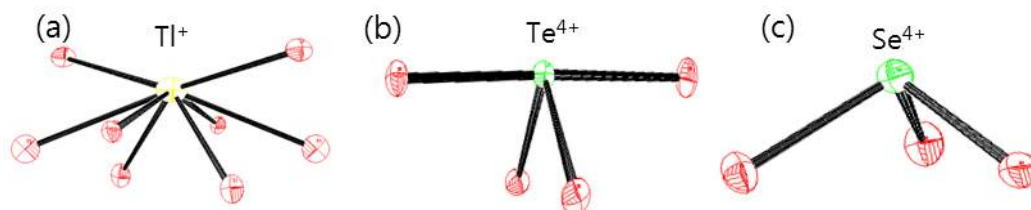


Figure 1.2 ORTEP (50% probability level ellipsoids) diagrams for asymmetric coordination environments of the lone-pair cations.

1.2 Hexagonal tungsten oxide (HTO)

The HTO materials motif of corner-sharing octahedra are of interest because of their structural diversity since various cations may substitute for W^{6+} as well as A cations^{10,11} ($A = Na^+, K^+, Rb^+, Tl^+$, etc.). The HTO-type structures have a tendency to be layered and we can find A cations between the layers.

The Halasyamani group divides the polar HTO-type oxides into two groups. For the Class 1, AO_3 lone-pair polyhedra ($A = Se^{4+}$ and Te^{4+}) are “capped” on both sides, whereas for the Class 2, AO_3 lone pair polyhedra are “capped” on one side (see Figure 1.3).¹²

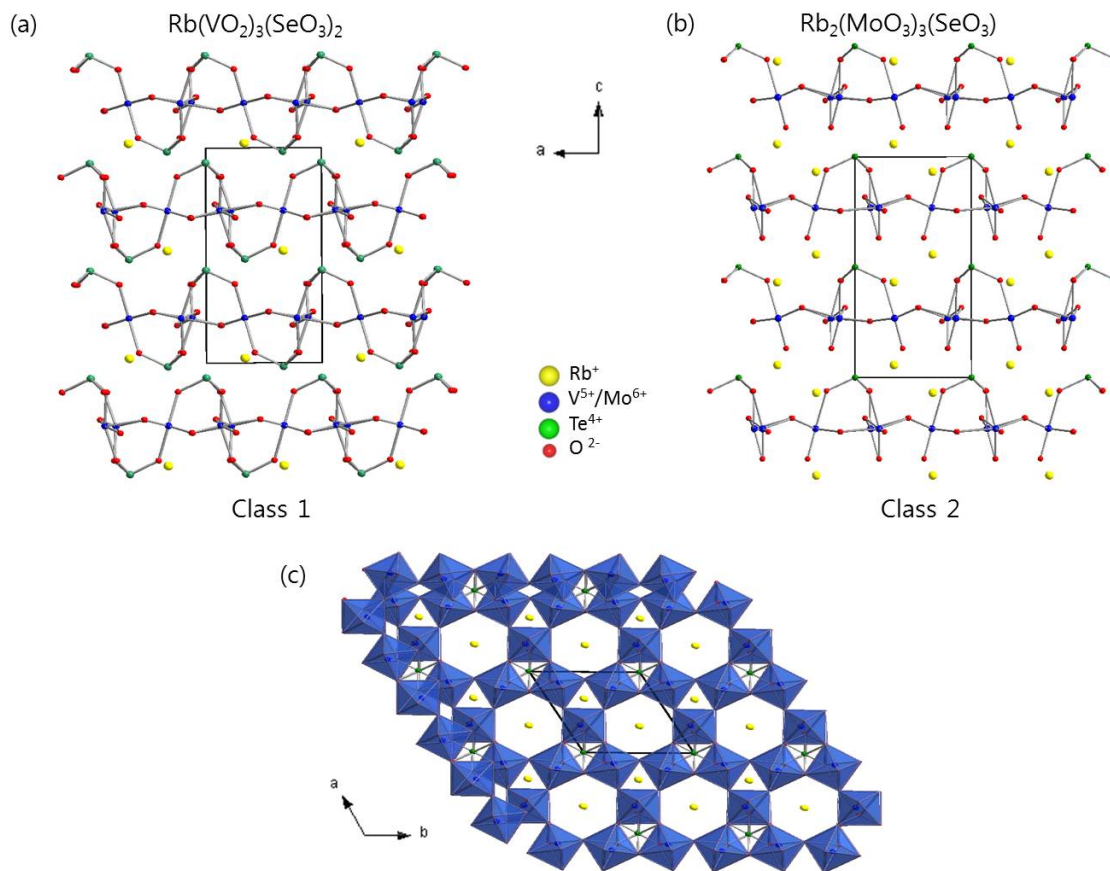


Figure 1.3 Ball-and-stick diagram of (a) $\text{Rb}(\text{VO}_2)_3(\text{SeO}_3)_2$ –HTO class 1, (b) $\text{Rb}_2(\text{MoO}_3)_3(\text{SeO}_3)$ –HTO class 2, and polyhedral diagram of (c) hexagonal tungsten oxide (HTO) topology¹²

Many groups studied HTO materials: Class 1 materials include $\text{A}(\text{VO}_2)_3(\text{SeO}_3)_2$ ($\text{A} = \text{NH}^{4+}$ or K^+ , Cs^+)^{13,14,15} by the Jacobson group; $\text{A}(\text{VO}_2)_3(\text{SeO}_3)_2$ ($\text{A} = \text{Rb}^+$, Tl^+)¹⁶ by the Halasyamani group; $\text{Cs}(\text{VO}_2)_3(\text{SeO}_3)_2$ ¹⁷ by the Buttery group. Class 2 materials include $\text{A}_2(\text{MoO}_3)_3(\text{SeO}_3)$ ($\text{A} = \text{NH}^{4+}$ or Cs^+)¹⁸, $\text{A}_2(\text{WO}_3)_3(\text{SeO}_3)$ ($\text{A} = \text{NH}^{4+}$ or Cs^+)¹⁹, $\text{A}_2(\text{MoO}_3)_3(\text{PO}_3\text{CH}_3)$ ($\text{A} = \text{Rb}^+$, Cs^+ or Tl^+)^{20,21} and $\text{Cs}_2(\text{WO}_3)_3(\text{PO}_3\text{CH}_3)$ ²² by the Jacobson group; $\text{A}_2(\text{MoO}_3)_3(\text{TeO}_3)$ ($\text{A} = \text{NH}^{4+}$ or Cs^+)²³ by the Vidyasagar group;

$A_2(\text{MoO}_3)_3(\text{SeO}_3)$ (A = Rb^+ or Tl^+),²⁴ $\text{Rb}_2(\text{WO}_3)_3(\text{TeO}_3)$,²⁵ and $\text{Na}_2(\text{WO}_3)_3(\text{SeO}_3)\cdot 2\text{H}_2\text{O}$ ²⁶ by the Halasyamani group.

One of our goals is synthesis and characterization of polar hexagonal tungsten oxide (HTO)-type materials as well as examination of their functional properties such as second-harmonic generation, piezoelectricity, pyroelectricity, and ferroelectricity.

1.3 References

1. Opik, U.; Pryce, M. H. L. *Proc. R. Soc. A.* **1957**, 238, 425.
2. Barder, R. F. W. *Mol. Phys.* **1960**, 3, 137.
3. Barder, R. F. W. *Can. J. Chem. Phys.* **1962**, 40, 2140.
4. Pearson, R. G. *J. Am. Chem. Soc.* **1969**, 91, 4947.
5. Pearson, R. G. *THEOCHEM* **1983**, 12, 25.
6. Wheeler, R. A.; Whangbo, M. H.; Hughbanks, T.; Hoffmann, R.; Burdett, J. K.; Albright, T. A. *J. Am. Chem. Soc.* **1986**, 108, 2222.
7. Halasyamani, P. S.; Poepelmeier, K. R. *Chem. Mater.* **1998**, 10, 2753.
8. Yeon, J. Dissertation: Synthesis, Characterization, Calculations, Functional properties, and Structure-property Relationships of New Mixed Metal Oxides, University of Houston, **2011**.
9. Chang, H. Y. Dissertation: Synthesis, Structures, Characterization, Calculations, and Functional Properties of New Mixed Oxides, University of Houston, **2009**.
10. Magneli, A. *Acta Chem. Scand.* **1953**, 7, 315.
11. Lee, K.-S.; D.-K., S.; Whangbo, M. -H. *J. Am. Chem. Soc.* **1997**, 119, 4043.
12. Chang, H. Y.; Kim, S. W.; Halasyamani, P. S. *Chem. Mater.* **2010**, 22, 3241.
13. Vaughey, J. T.; Harrison, W. T. A.; Dussack, L. L.; Jacobson, A. J. *Inorg. Chem.* **1994**, 33, 4370.
14. Harrison, W. T. A.; Dussack, L. L.; Jacobson, A. J. *Acta Crystallogr., Sect. C: Cryst. Struct. Commun.* **1995**, C51, 2473.

15. Harrison, W. T. A.; *Acta Crystallogr., Sect. C: Cryst. Struct. Commun.* **2000**, C56, 422.
16. Chang, H. Y.; Kim, S. W.; Ok, K. M.; Halasyamani, P. S. *Chem. Mater.* **2009**, 21, 1645.
17. Harrison, W. T. A.; Buttery, J. H. N. *Z. Anorg. Allg. Chem.* **2000**, 626, 867
18. Harrison, W. T. A.; Dussack, L. L.; Jacobson, A. J. *J. Inorg. Chem.* **1994**, 33, 6043.
19. Harrison, W. T. A.; Dussack, L. L.; Vogt, T.; Jacobson, A. J. *J. Solid State Chem.* **1995**, 120, 112.
20. Harrison, W. T. A.; Dussack, L. L.; Jacobson, A. J. *J. Inorg. Chem.* **1995**, 34, 4774.
21. Harrison, W. T. A.; Dussack, L. L.; Vogt, T.; Jacobson, A. J. *J. Solid State Chem.* **1998**, 138, 365.
22. Harrison, W. T. A.; Dussack, L. L.; Vaughey, J. T.; Vogt, T.; Jacobson, A. J. *J. Mater. Chem.* **1996**, 6, 81.
23. Balraj, V.; Vidyasagar, K. *J. Inorg. Chem.* **1998**, 37, 4764.
24. Chang, H. Y.; Kim, S. W.; Halasyamani, P. S. *Chem. Mater.* **2010**, 22, 3241
25. Goodey, J.; Ok, K. M.; Broussard, J.; Hofmann, C.; Escobedo, F. V.; Halasyamani, P. S. *J. Solid State Chem.* **2003**, 175, 3.
26. Nguyen, S. D.; Halasyamani, P. S. *Inorg. Chem.* **2013**, 52, 2637.

CHAPTER 2. Syntheses, Characterization, Functional Properties, and Structure-Property Relationships in Two New Oxides: $\text{Tl}_2\text{Cu}_2\text{Te}_7\text{O}_{17}$ and $\text{Tl}_2\text{Cu}_2\text{Te}_7\text{O}_{18}$

2.1 Abstract

Two new oxide materials, $\text{Tl}_2\text{Cu}_2\text{Te}_7\text{O}_{17}$ and $\text{Tl}_2\text{Cu}_2\text{Te}_7\text{O}_{18}$, have been synthesized by hydrothermal and solid-state techniques. The structures of $\text{Tl}_2\text{Cu}_2\text{Te}_7\text{O}_{17}$ and $\text{Tl}_2\text{Cu}_2\text{Te}_7\text{O}_{18}$ were determined by single crystal X-ray diffraction. The materials exhibit three-dimensional crystal structures consisting of corner- or edge-shared CuO_4 , CuO_5 , TeO_3 , TeO_4 , and TeO_5 polyhedra, and TeO_6 octahedra. $\text{Tl}_2\text{Cu}_2\text{Te}_7\text{O}_{17}$ crystallizes in a non-centrosymmetric and nonpolar space group, whereas $\text{Tl}_2\text{Cu}_2\text{Te}_7\text{O}_{18}$ crystallizes in a centrosymmetric and nonpolar space group. Powder second-harmonic generation (SHG) revealed a SHG efficiency of approximately $30 \times \alpha\text{-SiO}_2$. Piezoelectric experiments revealed d_{33} values of 13.4 pm/V. For the reported materials, infrared, UV-vis spectra, thermogravimetric, and differential thermal analysis were also presented. Crystal data: $\text{Tl}_2\text{Cu}_2\text{Te}_7\text{O}_{17}$, tetragonal, space group $P4_212$ (No. 90), $a = 8.8429(5) \text{ \AA}$, $b = 8.8429(5) \text{ \AA}$, $c = 12.2211(2) \text{ \AA}$, $V = 955.65(2) \text{ \AA}^3$, and $Z = 2$; $\text{Tl}_2\text{Cu}_2\text{Te}_7\text{O}_{18}$, monoclinic, space group $P2_1/n$ (No. 14), $a = 7.6005(6) \text{ \AA}$, $b = 11.8382(9) \text{ \AA}$, $c = 9.8379(8) \text{ \AA}$, $\beta = 90.9460(1)$, $V = 885.06(1) \text{ \AA}^3$, and $Z = 2$.

2.2 Introduction

Asymmetric cationic coordination environments in non-centrosymmetric (NCS) polar materials are of significant interest due to their technologically important properties such

as second-harmonic generation (SHG), piezoelectricity, ferroelectricity, and pyroelectricity.¹⁻⁴ Crystallographically, a material is considered polar if it crystallizes in one of ten polar crystal classes (1, 2, 3, 4, 6, m, mm2, 3m, 4mm, or 6mm).⁵ NCS materials may exhibit SHG and piezoelectricity, but ferroelectricity and/or pyroelectricity may be additionally observed for polar NCS materials. With respect to new materials, a number of design strategies have been discussed for creating new polar materials.⁵⁻¹³ We have focused on synthesizing new oxides containing cations susceptible to second-order Jahn-Teller (SOJT) distortions¹⁴⁻¹⁹ – octahedrally coordinated d^0 transition-metal cations (Ti^{4+} , V^{5+} , W^{6+} , Mo^{6+} , etc.) and cations with stereoactive lone-pairs (Se^{4+} , Te^{4+} , I^{5+} , Tl^+ , etc.) – which results in asymmetric coordination environments.

With respect to oxides that contain Tl^+ and Te^{4+} cations, a few compounds have been reported. For example β - $Tl_2[UO_2(TeO_3)_2]$ ²⁰ by the Albrecht-Schmitt group; $AgTlTeO_3$,²¹ by the Thomas group; $TlTeVO_5$,²² Tl_4CuTeO_6 , and $Tl_6CuTe_2O_{10}$ ²³ by the Halasyamani group. Of these materials, only $AgTlTeO_3$ and $TlTeVO_5$ are NCS and polar. β - $Tl_2[UO_2(TeO_3)_2]$, $TlTeVO_5$, Tl_4CuTeO_6 , and $Tl_6CuTe_2O_{10}$ crystallize in centrosymmetric structures with no second-harmonic generation (SHG) response. Various coordination environments for Cu^{2+} are observed, such as square planar, square pyramidal, and tetragonally distorted octahedral, attributable to first-order Jahn-Teller effects.²⁴ In expanding this research toward the synthesis of NCS material, we have successfully synthesized new oxides containing cations Cu^{2+} , as well as exhibiting TeO_3 , TeO_4 , and TeO_5 polyhedra in the same structure for $Tl_2Cu_2Te_7O_{17}$ and mixed valent tellurium Te^{4+} and Te^{6+} for $Tl_2Cu_2Te_7O_{18}$. The structure of $Tl_2Cu_2Te_7O_{17}$ is

centrosymmetric (CS) and nonpolar, whereas that of $\text{Tl}_2\text{Cu}_2\text{Te}_7\text{O}_{18}$ is non-centrosymmetric (NCS) and nonpolar.

In this chapter, we report the syntheses, characterization, functional properties, and structure-property relationships of $\text{Tl}_2\text{Cu}_2\text{Te}_7\text{O}_{17}$ and $\text{Tl}_2\text{Cu}_2\text{Te}_7\text{O}_{18}$. For $\text{Tl}_2\text{Cu}_2\text{Te}_7\text{O}_{17}$ we investigate its functional properties: second-harmonic generation (SHG) and piezoelectricity.

2.3 Experimental section

2.3.1 Synthesis

Tl_2CO_3 (Aldrich, 99.9+%), $\text{Cu}(\text{NO}_3)_2 \cdot 2.5\text{H}_2\text{O}$ (Alfa Aesar, 98+%), CuO (Alfa Aesar, 99%), TeO_2 (Aldrich, 99+%), and H_6TeO_6 (Aldrich, 99+%) were used as received.

Crystals of $\text{Tl}_2\text{Cu}_2\text{Te}_7\text{O}_{17}$ and $\text{Tl}_2\text{Cu}_2\text{Te}_7\text{O}_{18}$ were grown using hydrothermal techniques. 0.0549 g (0.171 mmol) of Tl_2CO_3 , 0.109 g (0.469 mmol) of $\text{Cu}(\text{NO}_3)_2 \cdot 2.5\text{H}_2\text{O}$, and 0.336 g (2.11 mmol) of TeO_2 for $\text{Tl}_2\text{Cu}_2\text{Te}_7\text{O}_{17}$ and 0.0606 g (0.129 mmol) of Tl_2CO_3 , 0.150 g (0.645 mmol) of $\text{Cu}(\text{NO}_3)_2 \cdot 2.5\text{H}_2\text{O}$, and 0.289 g (1.81 mmol) of TeO_2 for $\text{Tl}_2\text{Cu}_2\text{Te}_7\text{O}_{18}$, respectively, were combined with 4 mL of NH_4OH 1 M solution. The respective solutions were placed in 23 ml Teflon-lined autoclaves that were subsequently closed. The autoclave was heated to 230 °C, held for 2 days, and cooled slowly to room temperature at a rate of 6 °C/ h. The mother liquor was decanted from the products, and the products were recovered by filtration and washed with distilled water and acetone. Blue block-shaped crystals of $\text{Tl}_2\text{Cu}_2\text{Te}_7\text{O}_{17}$ and dark green plate-shaped crystals were obtained in ~10 % and ~20 % yield based upon TeO_2 .

Polycrystalline samples of $\text{Tl}_2\text{Cu}_2\text{Te}_7\text{O}_{17}$ and $\text{Tl}_2\text{Cu}_2\text{Te}_7\text{O}_{18}$ were prepared by conventional solid-state techniques. Stoichiometric amounts of Tl_2CO_3 (0.827 g, 1.76 mmol), CuO (0.275 g, 3.46 mmol), and TeO_2 (1.97 g, 12.3 mmol) for $\text{Tl}_2\text{Cu}_2\text{Te}_7\text{O}_{17}$, and Tl_2CO_3 (0.819 g, 1.75 mmol), CuO (0.278 g, 3.49 mmol), TeO_2 (1.67 g, 10.5 mmol), and H_6TeO_6 (0.401 g, 1.75 mmol) for $\text{Tl}_2\text{Cu}_2\text{Te}_7\text{O}_{18}$, were ground with an agate mortar and pressed into pellets. The pellets were placed in alumina crucibles and heated to 355 °C and 430 °C, respectively, in N_2 gas flowing for 2 days, and cooled to room temperature at 5 °C/min. In order to get the single phases, several intermediate grindings were essential. The purity of samples was monitored by powder X-ray diffraction.

2.3.2 Characterization

Single Crystal X-ray Diffraction. For $\text{Tl}_2\text{Cu}_2\text{Te}_7\text{O}_{17}$, a blue crystal ($0.08 \times 0.04 \times 0.04 \text{ mm}^3$) and for $\text{Tl}_2\text{Cu}_2\text{Te}_7\text{O}_{18}$, a dark green crystal ($0.06 \times 0.10 \times 0.16 \text{ mm}^3$), were used for single crystal X-ray diffraction data collection. Data were collected using a Siemens SMART diffractometer equipped with a 1K CCD area detector using graphite-monochromated $\text{Mo K}\alpha$ radiation. A hemisphere of data was collected using a narrow-frame method with scan widths of 0.30° in omega and an exposure time of 40 s per frame for both $\text{Tl}_2\text{Cu}_2\text{Te}_7\text{O}_{17}$ and $\text{Tl}_2\text{Cu}_2\text{Te}_7\text{O}_{18}$. The data were integrated using the Siemens SAINT program,²⁵ with the intensities corrected for Lorentz, polarization, air absorption, and absorption attributable to the variation in the path length through the detector faceplate. Psi-scans were used for the absorption correction on the hemisphere of data. The data were solved by direct methods using SHELXS-97 and refined using

SHELXL-97.^{26,27} All of the atoms were refined with anisotropic thermal parameters and converged for $I > 2\sigma(I)$. All calculations were performed using the WinGX-98 crystallographic software package.²⁸

Powder X-ray Diffraction. Powder X-ray diffraction (PXRD) data were collected using a PANalytical X'Pert PRO diffractometer at room temperature with Cu-K α radiation. The data were collected in the 2θ range of 5° - 70° in continuous scanning mode. No impurities were observed, and the experimental powder X-ray diffraction patterns are in good agreement with the calculated powder X-ray diffraction patterns.

Infrared (IR) Spectroscopy. Infrared spectra were recorded on a Matteson FT-IR 5000 spectrometer in the 400 – 4000 cm⁻¹ range.

UV-vis Diffuse Reflectance Spectroscopy. Diffuse reflectance spectra of polycrystalline powder samples of the reported materials were obtained using a Perkin Elmer Lambda 35 UV-vis scanning spectrophotometer equipped with an integrating sphere in the range 200 – 900 nm.

Thermal Analysis. Thermogravimetric analysis (TGA) and differential thermal analysis (DTA) were simultaneously carried out on EXSTAR TG/DTA 6300 series (SII Nano Technology Inc.). The samples (~20 mg) were placed in a platinum crucible that was heated and cooled between RT and 1000 °C at a rate of 10 °C/min under flowing nitrogen gas.

Second harmonic Generation (SHG). Powder SHG measurements were performed on a modified Kurtz –NLO system using a pulsed Nd:YAG laser with a wavelength of 1064 nm. A detailed description of the equipment and methodology has been published

elsewhere.⁵ The SHG efficiency has been shown to be dependent on particle size.²⁹ The $\text{Tl}_2\text{Cu}_2\text{Te}_7\text{O}_{17}$ material was ground and sieved into distinct particle size ranges (<20, 20-45, 45-63, 63-75, 75-90, >90 μm). To make relevant comparisons with known SHG materials, crystalline $\alpha\text{-SiO}_2$ and LiNbO_3 were ground and sieved into the sample particle size ranges.

Piezoelectric Measurements. Converse piezoelectric measurements were performed using a Radiant Technologies RT66A piezoelectric test system with a TREK high voltage amplifier, Precision Materials Analyzer, Precision High Voltage Interface, and MTI 2000 Fotonic Sensor. $\text{Tl}_2\text{Cu}_2\text{Te}_7\text{O}_{17}$ sample was pressed into pellet (~1 cm diameter, ~1 mm thick) and sintered at 355 °C for 2 days. Silver paste was applied to both sides of the pellet, and the pellet was cured at 300 °C for 12h.

2.4 Results and discussion

Structures. $\text{Tl}_2\text{Cu}_2\text{Te}_7\text{O}_{17}$ exhibits a three-dimensional (3D) structure consisting of corner-shared CuO_4 , CuO_5 , TeO_3 , TeO_4 , and TeO_5 , polyhedra that run along the b -axis direction (see Figure 2.1(a)). Corner-shared Te(1)O_3 and Te(2)O_4 polyhedra form a one-dimensional chain along the c -axis, and these chains are further connected by Te(3)O_5 polyhedra along the a -axis. The CuO_4 and CuO_5 polyhedra alternate in the layer and are corner-shared to Te(1)O_3 , Te(2)O_4 and Te(3)O_5 polyhedra, resulting in the three-dimensional structure (see Figure 2.1(b)). In connectivity terms, the structure can be described as $\{[\text{Cu(1)O}_{4/2}]^{2-} [\text{Cu(2)O}_{5/2}]^{3-} 4[\text{Te(1)O}_{3/2}]^+ 2[\text{Te(2)O}_{4/2}]^0 [\text{Te(3)O}_{5/2}]^-\}^{2-}$, with

charge balance maintained by two Tl^+ cations. For the CuO_4 polyhedra, the Cu^{2+} cation is in square planar coordination environments bonded to four oxygen atoms with a Cu–O bond distance of 1.925(4) Å. The Cu–O bond distances in CuO_5 polyhedra range between 1.934(4) and 2.210(8) Å. One of the most interesting aspects of $\text{Tl}_2\text{Cu}_2\text{Te}_7\text{O}_{17}$ is the occurrence of all three TeO_3 , TeO_4 , and TeO_5 . Te–O bond distances range from 1.812(8) to 2.151(4) Å. The Te^{4+} cations are in asymmetric coordination environments attributable to their stereo-active lone-pair. The Tl^+ cation is surrounded by eight oxygen atoms with Tl–O distances ranging from 2.822(4) to 3.371(2) Å. The bond valence calculations^{31,32} for Cu^{2+} , Te^{4+} , and Tl^+ resulted in values of 2.056–2.246, 3.825–4.062, and 0.962, respectively. Detailed bond valences for $\text{Tl}_2\text{Cu}_2\text{Te}_7\text{O}_{17}$ are shown in Table 2.6. $\text{Tl}_2\text{Cu}_2\text{Te}_7\text{O}_{18}$ exhibits a three-dimensional (3D) structure consisting of corner-shared CuO_4 , TeO_3 , and TeO_4 polyhedra and TeO_6 octahedra, which run along the *c*-axis direction (see Figure 2.2(a)). Edge-shared Te(2)O_4 polyhedra are connected via corner-sharing by Te(3)O_4 polyhedra and Te(1)O_6 octahedra. The CuO_4 polyhedra in the layer are corner-shared to Te(3)O_4 and Te(4)O_3 polyhedra (see Figure 2.2(b)). In connectivity terms, the structure can be described as $\{2[\text{Cu(1)O}_{4/2}]^{2-} [\text{Te(1)O}_{6/2}]^0 2[\text{Te(2)O}_{4/2}]^0 2[\text{Te(3)O}_{4/2}]^0 2[\text{Te(4)O}_{3/2}]^+\}^{2-}$, with charge balance maintained by two Tl^+ cations. There are two crystallographically unique tellurium sites, Te(1) represents Te^{6+} and Te(2) – Te(4) represent Te^{4+} . The Te^{6+} cation is in an octahedral coordination environment bonded to six oxygen atoms, with Te–O bond distances ranging from 1.897(3) to 1.955(3) Å. The Te^{4+} cations are in seesaw and distorted trigonal pyramidal environments, with Te–O bond distances ranging from 1.873(4) to 2.198(4) Å. The Te^{4+}

cations are in asymmetric coordination environments attributable to their lone pair. The Cu^{2+} cation is in a square planar coordination environment bonded to four oxygen atoms, with Cu–O bond distances ranging from 1.950(4) to 1.958(4) Å. The Tl^+ cation is surrounded by eight oxygen atoms with Tl–O distances ranging from 2.811(4) to 3.442(4) Å. The bond valence calculations^{31,32} for Cu^{2+} , Te^{6+} , Te^{4+} , and Tl^+ resulted in values of 1.905, 5.800, 3.700–3.895, and 0.879, respectively. Detailed bond valances for $\text{Tl}_2\text{Cu}_2\text{Te}_7\text{O}_{18}$ are shown in Table 2.7. The local coordination environments of the reported materials are shown in Figure 2.3.

Bulk Polycrystalline. Polycrystalline samples of $\text{Tl}_2\text{Cu}_2\text{Te}_7\text{O}_{17}$ and $\text{Tl}_2\text{Cu}_2\text{Te}_7\text{O}_{18}$ were prepared by conventional solid-state techniques. Powder patterns of reported materials were provided as Figure 2.4. We observed impurity peaks from the experiment of $\text{Tl}_2\text{Cu}_2\text{Te}_7\text{O}_{17}$ that reveals CuTe_2O_5 . Almost all peaks from the experiment of $\text{Tl}_2\text{Cu}_2\text{Te}_7\text{O}_{18}$ are well matched to the corresponding calculated powder pattern.

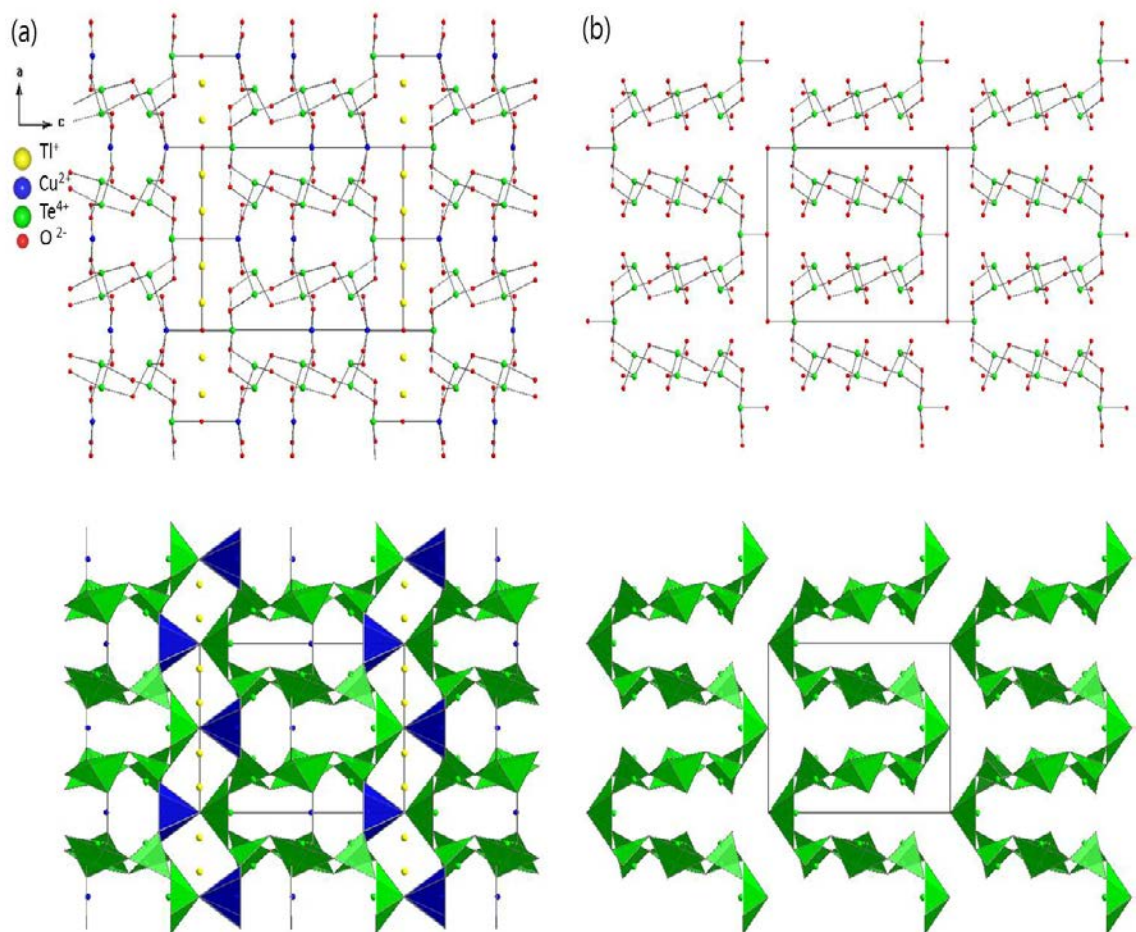


Figure 2.1 Ball-and-stick and polyhedral diagram of $Tl_2Cu_2Te_7O_{17}$ in the ac -plane consisting of the TeO_3 , TeO_4 , and TeO_5 polyhedra (a) with and (b) without CuO_4 , CuO_5 polyhedra and Tl^+ cations.

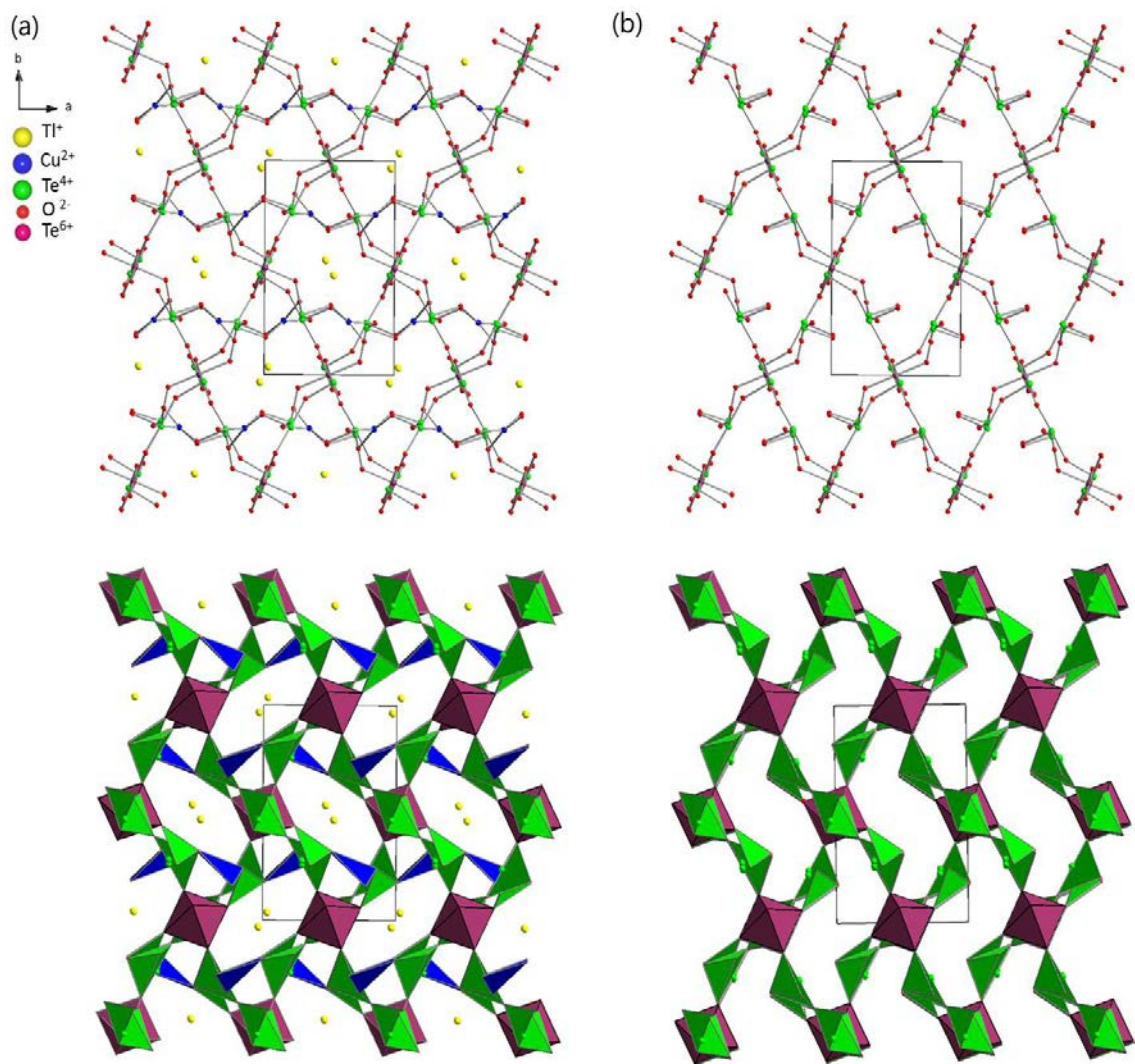


Figure 2.2 Ball-and-stick and polyhedral diagram of $Tl_2Cu_2Te_7O_{18}$ in the ab -plane consisting of the TeO_3 , TeO_4 , and TeO_6 polyhedra (a) with and (b) without CuO_4 polyhedra and Tl^+ cations.

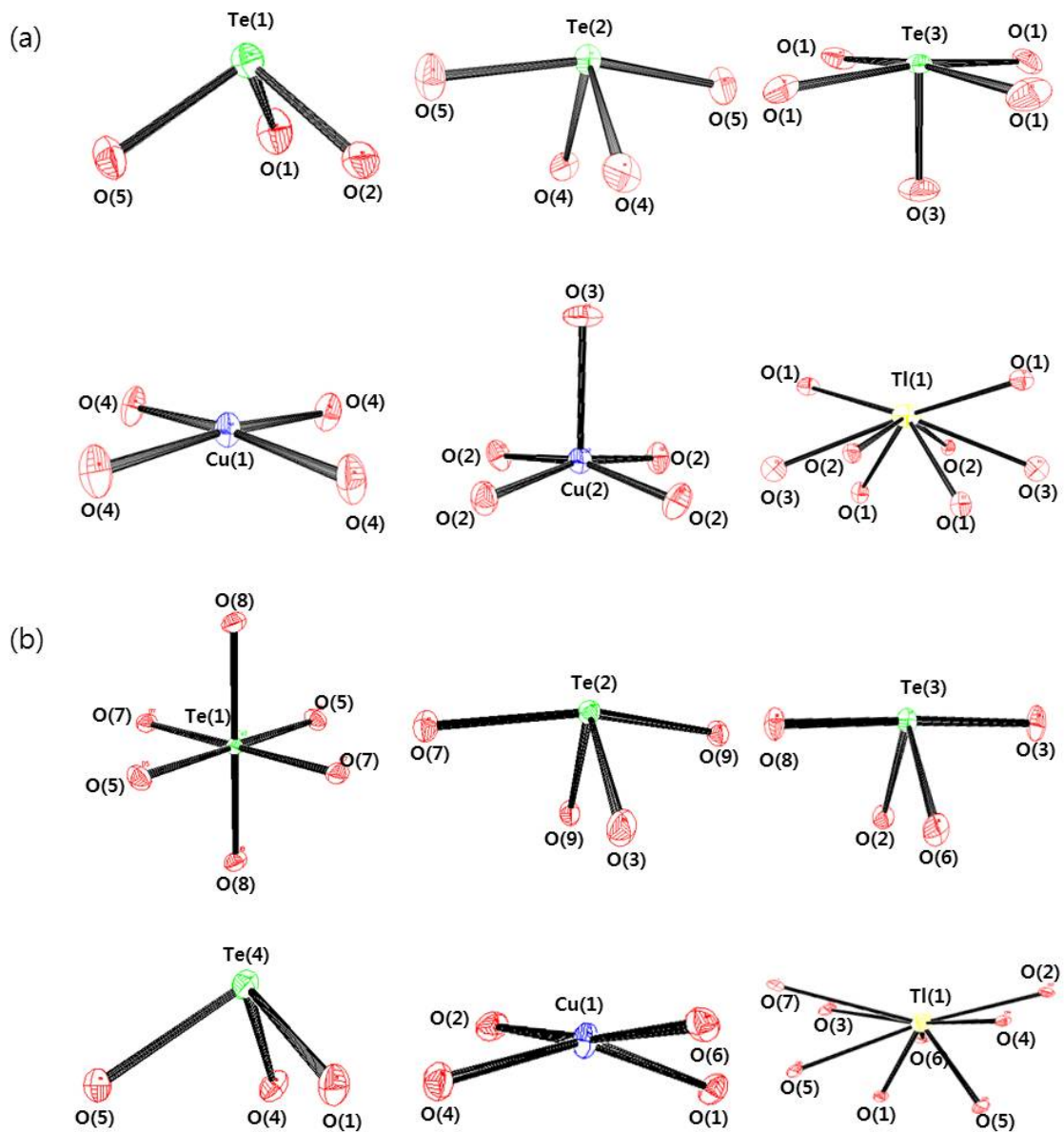


Figure 2.3 ORTEP (50% probability level ellipsoids) diagrams for (a) $\text{Tl}_2\text{Cu}_2\text{Te}_7\text{O}_{17}$ and (b) $\text{Tl}_2\text{Cu}_2\text{Te}_7\text{O}_{18}$.

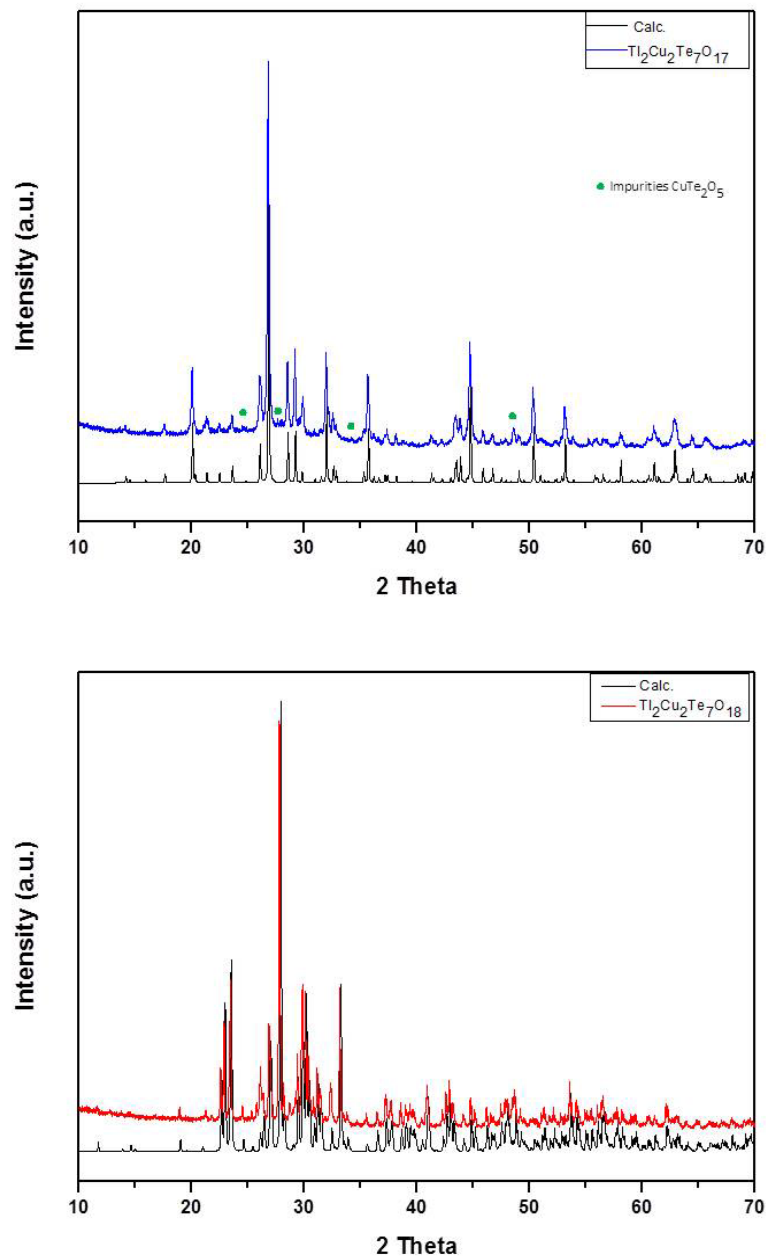
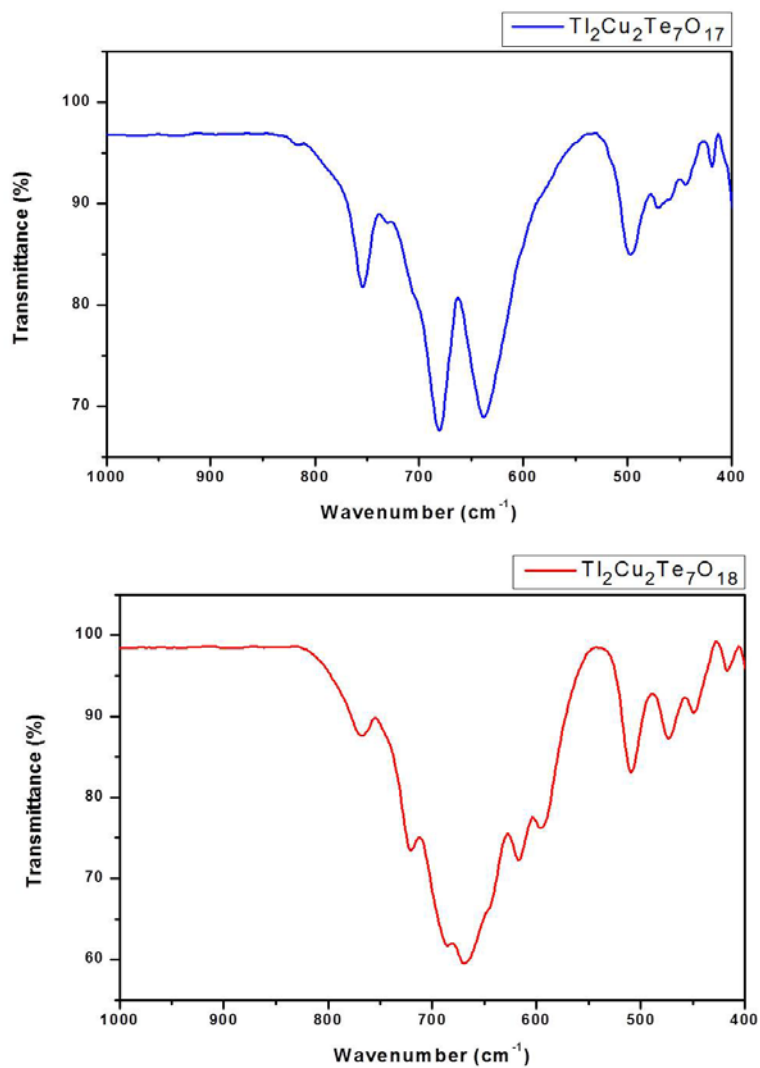


Figure 2.4 Calculated and observed powder X-ray diffraction pattern for $\text{Tl}_2\text{Cu}_2\text{Te}_7\text{O}_{17}$ and $\text{Tl}_2\text{Cu}_2\text{Te}_7\text{O}_{18}$.

Infrared Spectroscopy. The infrared spectra of the two compounds, $\text{Tl}_2\text{Cu}_2\text{Te}_7\text{O}_{17}$ and $\text{Tl}_2\text{Cu}_2\text{Te}_7\text{O}_{18}$, revealed Te-O, Te-O-Te, and Cu-O vibrations between 400 and 1000 cm^{-1} . The peaks in the 680 – 768 cm^{-1} range can be attributed to Te^{4+} -O stretching vibrations, whereas the bands in the 669 – 671 cm^{-1} range and peaks at 594 cm^{-1} can be assigned to Te^{6+} -O symmetric and antisymmetric stretching vibrations (i.e. $\text{Tl}_4\text{CuTe}^{6+}\text{O}_6$ ²³ and $\text{Rb}_4[\text{Te}_5^{6+}\text{Te}_3^{4+}]\text{O}_{23}$ ³³). The remaining bands in the spectrum are likely attributed to Te-O-Te bending vibrations³³ or Cu-O vibrations (i.e. $\text{Pb}_2\text{Cu}_3\text{B}_4\text{O}_{11}$ ³⁴). The IR spectra and assignments are shown in Figure 2.5.



	$\text{Tl}_2\text{Cu}_2\text{Te}_7\text{O}_{17}$	$\text{Tl}_2\text{Cu}_2\text{Te}_7\text{O}_{18}$
$\nu (\text{Te}^{4+}\text{-O})$	755, 680	768, 721, 685
$\nu (\text{Te}^{6+}\text{-O})$		669, 671
$\nu_{\text{anti.}} (\text{Te}^{6+}\text{-O})$		594
$\delta (\text{Te-O-Te})$ or $\nu (\text{Cu-O})$	471, 456, 419	498, 473, 448, 417

Figure 2.5 IR data and assignments for $\text{Tl}_2\text{Cu}_2\text{Te}_7\text{O}_{17}$ and $\text{Tl}_2\text{Cu}_2\text{Te}_7\text{O}_{18}$.^{23,33,34}

UV-vis Diffuse Reflectance Spectroscopy. $\text{Tl}_2\text{Cu}_2\text{Te}_7\text{O}_{17}$ is blue, whereas $\text{Tl}_2\text{Cu}_2\text{Te}_7\text{O}_{18}$ is dark green. The UV-vis diffuse reflectance spectra indicate that the absorption energy for the materials is approximately over 2.2 eV. Absorption (K/S) data were calculated from the Kubelka-Munk function³⁵ :

$$F(R) = \frac{(1-R)^2}{2R} = \frac{K}{S}$$

with R representing the reflectance, K the absorption, and S the scattering. In a K/S versus E (eV) plot, extrapolating the linear part of the rising curve to zero provides the onset of absorption at 2.86 eV for $\text{Tl}_2\text{Cu}_2\text{Te}_7\text{O}_{17}$, and 2.43 eV for $\text{Tl}_2\text{Cu}_2\text{Te}_7\text{O}_{18}$. The UV-Vis diffuse reflectance spectra for the reported materials are shown in Figure 2.6.

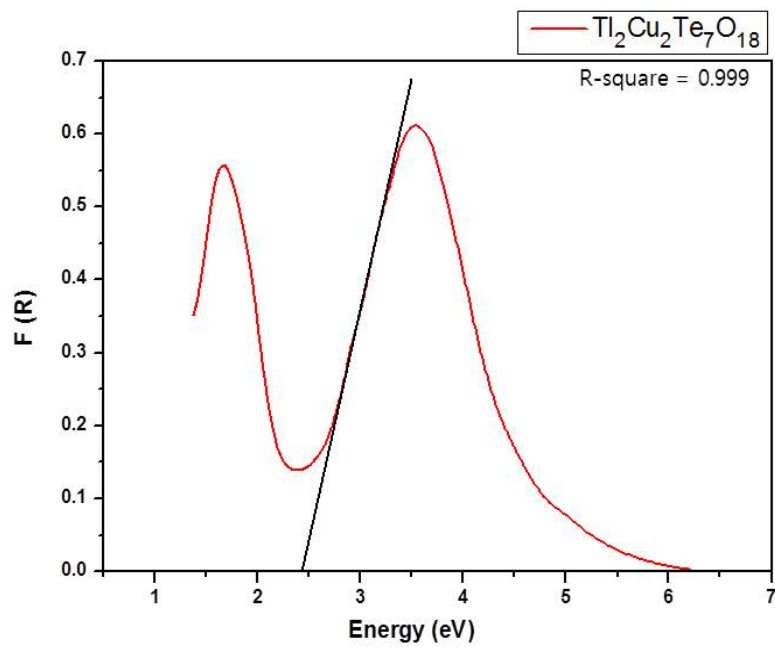
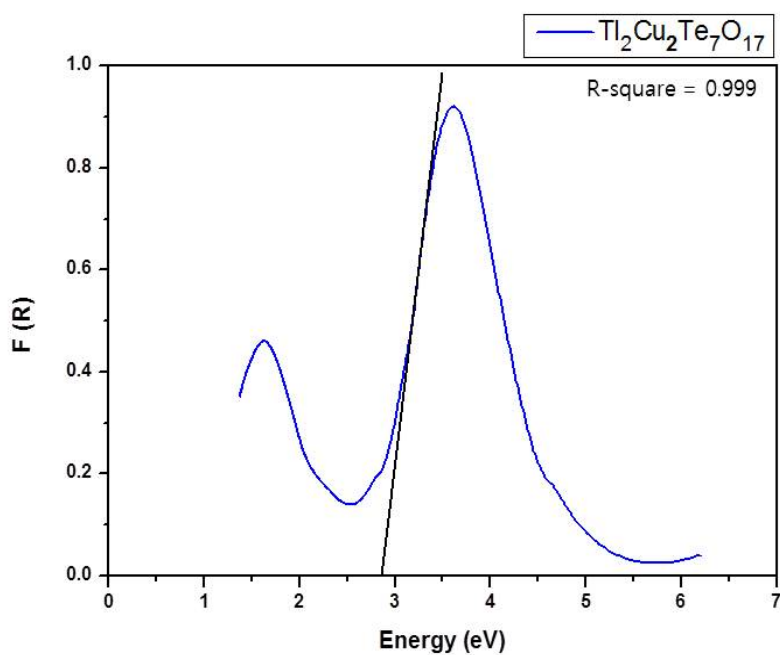


Figure 2.6 UV-vis diffuse reflectance spectroscopy data for $\text{Tl}_2\text{Cu}_2\text{Te}_7\text{O}_{17}$ and $\text{Tl}_2\text{Cu}_2\text{Te}_7\text{O}_{18}$.

Thermal Analysis. The thermal behaviors of the reported materials have been investigated using thermogravimetric analysis (TGA) and differential thermal analysis (DTA) measurements. Both TGA and DTA curves were measured under flowing N₂ gas from room temperature to 1000 °C. As seen in the TGA, no weight loss was observed up to 600 °C, but endothermic peaks found above 400 °C in the heating cycles of DTA data indicate the materials melt incongruently (see Figure 2.7). The thermal decomposition products at 600 °C were CuTe₂O₅³⁶ for Tl₂Cu₂Te₇O₁₇, and Cu₃TeO₆³⁷ and TeO₂³⁸ for Tl₂Cu₂Te₇O₁₈, respectively, as confirmed by Powder X-ray diffraction measurements (see Figure 2.8).

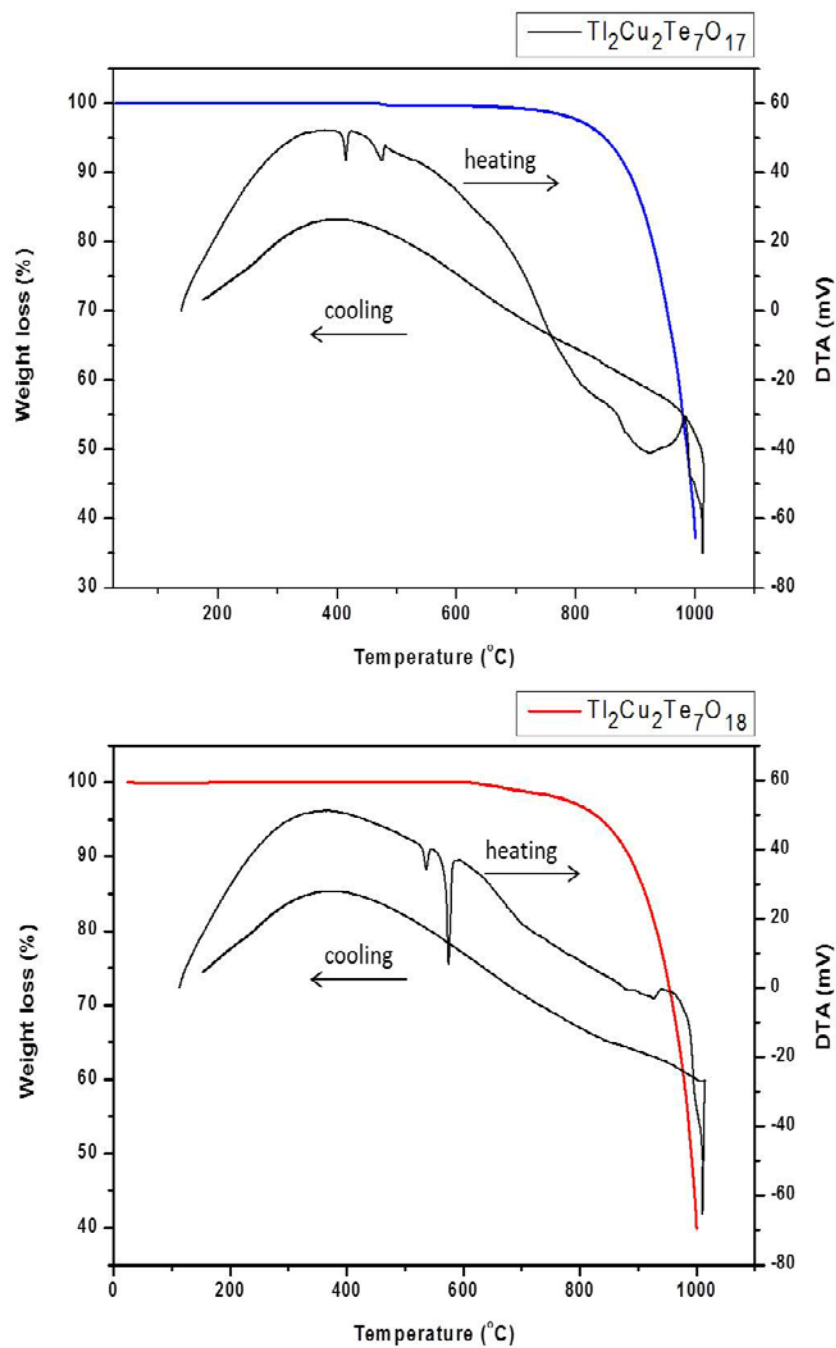


Figure 2.7 Thermogravimetric analysis (TGA) and differential thermal analysis (DTA) diagram for $\text{Tl}_2\text{Cu}_2\text{Te}_7\text{O}_{17}$ and $\text{Tl}_2\text{Cu}_2\text{Te}_7\text{O}_{18}$.

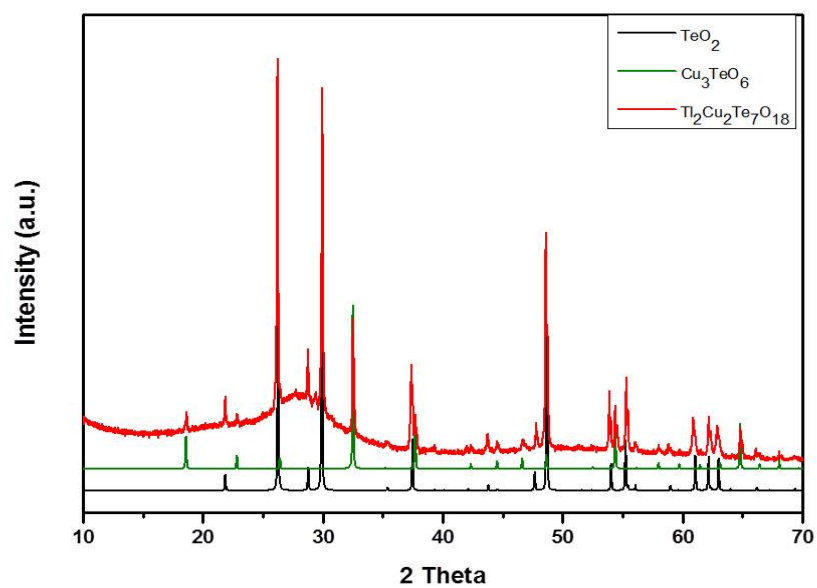
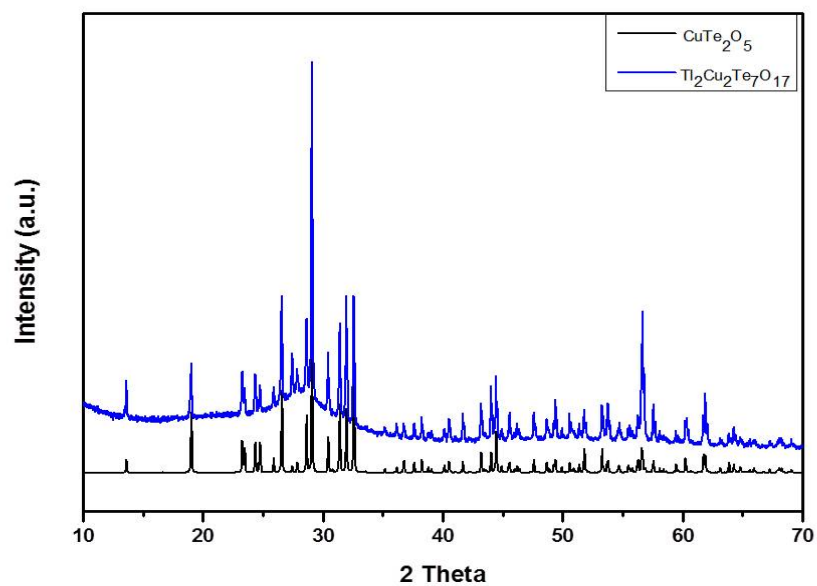


Figure 2.8 Powder X-ray diffraction data of residues for $\text{Tl}_2\text{Cu}_2\text{Te}_7\text{O}_{17}$ and $\text{Tl}_2\text{Cu}_2\text{Te}_7\text{O}_{18}$.

Second harmonic Generation (SHG) and Piezoelectricity. Because $\text{Tl}_2\text{Cu}_2\text{Te}_7\text{O}_{17}$ crystallizes in a non-centrosymmetric (NCS) space group, $P42_12$, SHG and piezoelectric measurements were carried out. Powder SHG measurements using 1064 nm radiation revealed that $\text{Tl}_2\text{Cu}_2\text{Te}_7\text{O}_{17}$ has SHG efficiency of approximately $30 \times \alpha\text{-SiO}_2$ in the 45 ~ 63 μm particle size range. Additional SHG measurements with various particle sizes, ranging from 20 to 125 μm , indicate that the reported material exhibits non-phase matching (see Figure 2.9). Based on the SHG efficiencies and phase-matching measurements, the material falls into the class C category of SHG materials, as defined by Kurtz and Perry.²⁹ The average NLO susceptibility $\langle d_{\text{eff}} \rangle_{\text{exp}}$ was determined to be ~ 3.0 pm/V.⁵ Also, converse piezoelectric measurements were performed on the reported material. A maximum voltage of 1000V was applied and 20 measurements were performed and averaged. The value of the piezoelectric charge constant, d_{33} , can be calculated from:

$$L = SL_0 \sim Ed_{33}L_0$$

Where L is the displacement of the sample, L_0 is the sample thickness (m), S is the strain (L/L_0), and E is the electric field strength (V/m).³⁹ The d_{33} piezoelectric charge constant of 13.4 pm/V for $\text{Tl}_2\text{Cu}_2\text{Te}_7\text{O}_{17}$ was estimated (see Figure 2.10).

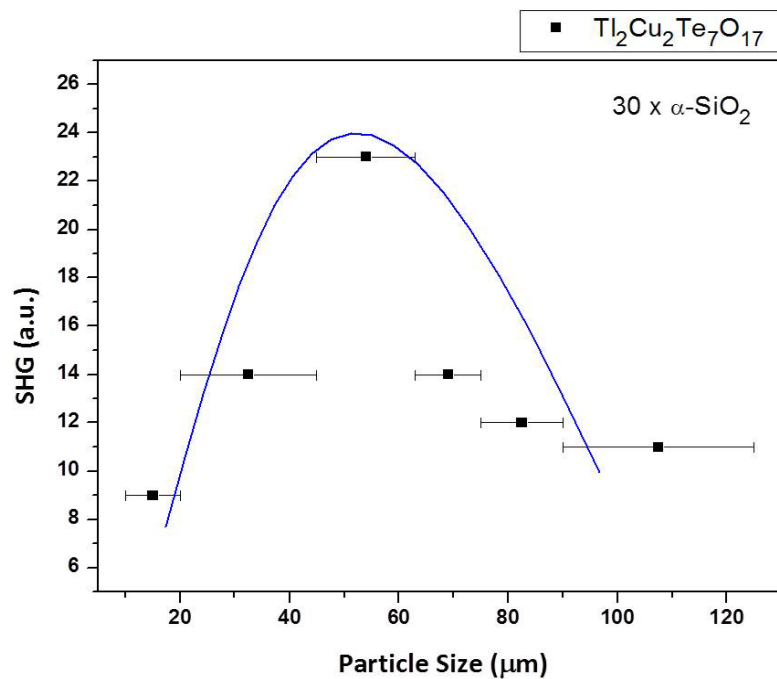


Figure 2.9 Powder second-harmonic generation for $\text{Tl}_2\text{Cu}_2\text{Te}_7\text{O}_{17}$.

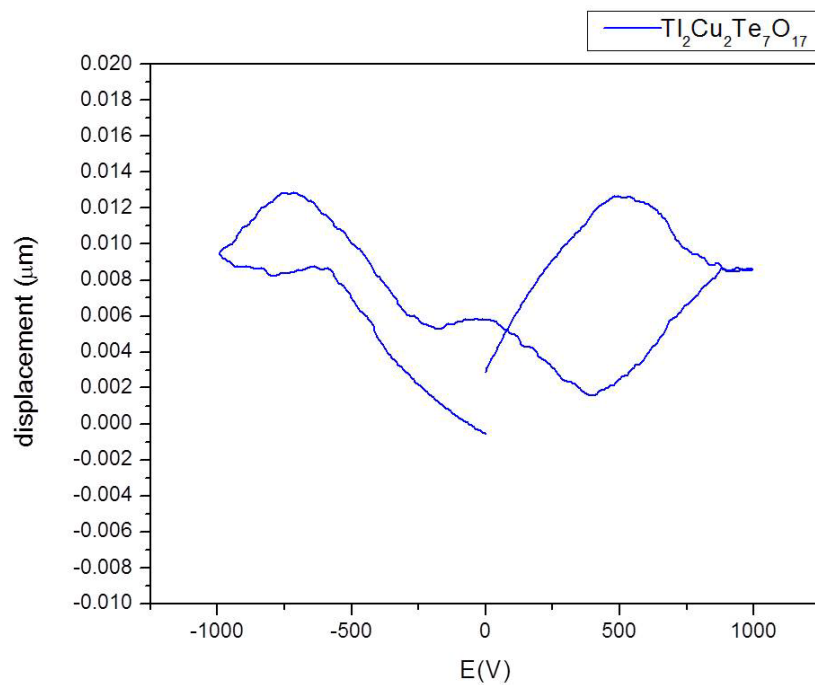


Figure 2.10 Displacement vs. electric field loops for $\text{Tl}_2\text{Cu}_2\text{Te}_7\text{O}_{17}$.

2.5 Conclusion

We have successfully synthesized and characterized two new oxide materials, $\text{Tl}_2\text{Cu}_2\text{Te}_7\text{O}_{17}$ and $\text{Tl}_2\text{Cu}_2\text{Te}_7\text{O}_{18}$. Crystals and polycrystalline powders were synthesized by hydrothermal and conventional solid-state techniques, respectively. Both materials exhibit three-dimensional structures. $\text{Tl}_2\text{Cu}_2\text{Te}_7\text{O}_{17}$ is non-centrosymmetric and crystallizes in the *nonpolar* acentric space group $P42_12$, whereas $\text{Tl}_2\text{Cu}_2\text{Te}_7\text{O}_{18}$ is centrosymmetric and crystallizes in the *nonpolar* centrosymmetric space group $P2_1/n$. $\text{Tl}_2\text{Cu}_2\text{Te}_7\text{O}_{17}$ exhibits SHG efficiency of approximately $30 \times \alpha\text{-SiO}_2$. We are currently in the process of scaling up the synthesis for magnetic measurement experiments, as well as expanding into the other lone-pair cation and magnetic cation oxide system.

2.6 References

1. Nye, J. *Physical Properties of Crystals*; Oxford University Press: Oxford, **1957**.
2. Cady, W.G. *Piezoelectricity; an Introduction to the Theory and Applications of Electromechanical Phenomena in Crystals*; Dover: New York, **1964**.
3. Jona, F.; Shirane, G. *Ferroelectric Crystals*; Pergamon Press: Oxford, **1962**.
4. Lang, S. B. *Sourcebook of Pyroelectricity*; Gordon & Breach: London, **1974**.
5. Ok, K.; Chi, E.; Halasyamani, P. *Chem. Soc. Rev.* **2006**, *35*, 710.
6. Yeon, J.; Kim, S.-H.; Nguyen, S. D.; Lee, H.; Halasyamani, P. S. *Inorg. Chem.* **2012**, *51*, 609.
7. Welk, M. E.; Norquist, A. J.; Stern, C. L.; Poeppelmeier, K. R. *Inorg. Chem.* **2001**, *40*, 5479.
8. Welk, M. E.; Norquist, A. J.; Arnold, F. P.; Stern, C. L.; Poeppelmeier, K. R. *Inorg. Chem.* **2002**, *41*, 5119.
9. Izumi, H. K.; Kirsch, J. E.; Stern, C. L.; Poeppelmeier, K. R. *Inorg. Chem.* **2005**, *44*, 884.
10. Muller, E. A.; Cannon, R. J.; Sarjeant, A. N.; Ok, K. M.; Halasyamani, P. S.; Norquist, A. J. *J. Cryst. Growth Des.* **2005**, *5*, 1913.
11. Veltman, T. R.; Stover, A. K.; Sarjeant, A. N.; Ok, K. M.; Halasyamani, P. S.; Norquist, A. J. *Inorg. Chem.* **2006**, *45*, 5529.
12. Yeon, J.; Kim, S.-H.; Nguyen, S. D.; Lee, H.; Halasyamani, P. S. *Inorg. Chem.* **2012**, *51*, 2662.

13. Leblanc, N.; Mercier, N.; Zorina, L.; Simonov, S.; Auban-Senzier, P.; Pasquier, C. *J. Am. Chem. Soc.* **2011**, 133, 14924.
14. Opik, U.; Pryce, M. H. L. *Proc. R. Soc. A.* **1957**, 238, 425.
15. Barder, R. F. W. *Mol. Phys.* **1960**, 3,137.
16. Barder, R. F. W. *Can. J. Chem. Phys.* **1962**, 40, 2140.
17. Pearson, R. G. *J. Am. Chem. Soc.* **1969**, 91, 4947.
18. Pearson, R. G. *THEOCHEM* **1983**, 12, 25.
19. Wheeler, R. A.; Whangbo, M. H.; Hughbanks, T.; Hoffmann, R.; Burdett, J. K.; Albright, T. A. *J. Am. Chem. Soc.* **1986**, 108, 2222.
20. Almond P. M.; Albrecht-Schmitt, T. E. *Inorg. Chem.* **2002**, 41, 5495.
21. Linda, D.; Dutreilh-Colas, M.; Loukil, M.; Mirgorodsky, A.; Masson, O.; Duclere, J. R.; Thomas, P.; Kabadou, A. *Mater. Res. Bull.* **2010**, 45, 1883.
22. Sivakumar, T.; Chang, H. -Y.; Baek, J.; Halasyamani, P. S. *Chem. Mater.* **2007**, 19, 4710.
23. Yeon, J.; Kim, S.-H.; Green, M.; Bhatti, K.; Leighton, C. Halasyamani, P. S. *J. Solid State Chem.* **2012**, 196, 607.
24. Jahn, H. A.; Teller, E. *Proc. R. Soc. London, Ser. A* **1937**, 161, 220.
25. SAINT: *A Program for Area Detector Absorption Correction*, Version 4.05; Siemens Analytical X-ray Systems, Inc.: Madison, WI, **1995**.
26. Sheldrick, G. M. *SHELXS-97 - A Program for Crystal Structure Refinement*; University of Goettingen: Goettingen, Germany, **1997**.

27. Sheldrick, G. M. *SHELXL-97 - A Program for Automatic Solution of Crystal Structures*. University of Goettingen: Goettingen, Germany, **1997**.
28. Farrugia, L. J. *J. Appl. Crystallogr.* **1999**, *32*, 837.
29. Kurtz, S.; Perry, T. *J. Appl. Phys.* **1968**, *39*, 3798.
30. Yeon, J.; Kim, S.-H.; Hayward, M. A.; Halasyamani, P. S. *Inorg. Chem.* **2011**, *50*, 8663.
31. Brown, I. D.; Altermatt, D. *Acta Crystallogr., Sect. B* **1985**, *B41*, 244.
32. Brown, I. D. *The Chemical Bond in Inorganic Chemistry*; Oxford University Press: New York, **2012**; Vol. *12*.
33. Minimol, M. P.; Vidyasagar, K. *Inorg. Chem.* **2005**, *44*, 9369.
34. Pan, S.; Watkins, B.; Smit, J. P.; Marvel, M. R.; Saratovsky, I.; Poepelmeier, K. R. *Inorg. Chem.* **2007**, *46*, 3851.
35. Kubelka, P.; Munk, F. Z. *Tech. Phys.* **1931**, *12*, 593.
36. Hanke, K.; Kupcik, V.; Lindqvist, O. *Acta Crystallogr., Sect. B* **1973**, *29*, 963.
37. Flack, L.; Lindqvist, O.; Moret, J. *Acta Crystallogr., Sect. B* **1978**, *34*, 896.
38. Worlton, T. G.; Beyerlein, R. A. *Phys. Rev. B* **1975**, *12*, 1899.
39. Chang, H. Y. Dissertation: Synthesis, Structures, Characterization, Calculations, and Functional properties of New Mixed Oxides, University of Houston, **2009**.

Table 2.1 Crystallographic data for $\text{Tl}_2\text{Cu}_2\text{Te}_7\text{O}_{17}$ and $\text{Tl}_2\text{Cu}_2\text{Te}_7\text{O}_{18}$.

formula	$\text{Tl}_2\text{Cu}_2\text{Te}_7\text{O}_{17}$	$\text{Tl}_2\text{Cu}_2\text{Te}_7\text{O}_{18}$
fw	1701.05	1717.05
T(K)	296.0(2)	296.0(2)
crystal system	Tetragonal	Monoclinic
space group	$P 4 2_1 2$ (No. 90)	$P 2_1/n$ (No. 14)
a (Å)	8.8429(5)	7.6005(6)
b (Å)	8.8429(5)	11.8382(9)
c (Å)	12.2211(2)	9.8379(8)
α (deg)	90	90
β (deg)	90	90.9460(1)
γ (deg)	90	90
V (Å ³)	955.65(2)	885.06(1)
Z	2	2
ρ_{calcd} (g/cm ³)	5.911	6.443
R (int)	0.0496	0.0235
GOF (F^2)	1.122	1.093
$R(F)^a$	0.0200	0.0195
$R_w(F_o^2)^b$	0.0502	0.0421

$$^a R(F) = \frac{\sum ||F_o| - |F_c||}{\sum |F_o|}, \quad ^b R_w(F_o^2) = [\sum w(F_o^2 - F_c^2)^2 / \sum w(F_o^2)^2]^{1/2}$$

Table 2.2 Atomic coordinates and equivalent isotropic displacement parameters (\AA^2) for $\text{Tl}_2\text{Cu}_2\text{Te}_7\text{O}_{17}$.

	x	y	z	U_{eq}^a
Tl(1)	0.6493(3)	0.3507(3)	0	0.036(1)
Te(1)	0.3050(4)	0.3175(4)	0.7389(3)	0.015(1)
Te(2)	0.1854(3)	0.1854(3)	1/2	0.013(1)
Te(3)	1/2	0	0.8496(6)	0.013(2)
Cu(1)	1/2	0	0.4552(1)	0.013(3)
Cu(2)	1/2	0	0.1788(1)	0.015(3)
O(1)	0.3941(5)	0.2184(5)	0.8607(3)	0.022(9)
O(2)	0.1134(5)	0.3152(5)	0.8006(3)	0.020(9)
O(3)	1/2	0	0.9979(7)	0.028(2)
O(4)	0.3151(4)	0.8856(4)	0.4478(3)	0.017(9)
O(5)	0.2736(5)	0.1377(4)	0.6552(3)	0.019(8)

^a U_{eq} is defined as one third of the trace of the orthogonalized U_{ij} tensor.

Table 2.3 Atomic coordinates and equivalent isotropic displacement parameters (\AA^2) for $\text{Tl}_2\text{Cu}_2\text{Te}_7\text{O}_{18}$.

	x	y	z	U_{eq}^a
Tl(1)	0.4682(4)	0.5358(2)	0.7583(3)	0.033(9)
Te(1)	0	1/2	0	0.008(1)
Te(2)	0.0353(4)	0.5341(3)	0.3461(3)	0.010(8)
Te(3)	0.2085(4)	0.7572(3)	0.9562(3)	0.010(8)
Te(4)	0.2895(4)	0.2803(3)	0.9434(3)	0.009(8)
Cu(1)	0.1491(8)	0.2509(5)	0.2448(6)	0.011(1)
O(1)	0.5121(5)	0.3243(3)	0.8842(4)	0.014(8)
O(2)	0.2300(5)	0.8414(3)	0.1156(4)	0.012(7)
O(3)	0.8204(5)	0.6109(3)	0.3263(4)	0.014(8)
O(4)	0.3524(5)	0.2566(3)	0.1256(4)	0.012(7)
O(5)	0.2379(5)	0.4387(3)	0.9866(4)	0.013(8)
O(6)	0.5131(5)	0.3140(3)	0.5942(4)	0.014(8)
O(7)	0.0270(5)	0.5679(3)	0.8222(4)	0.012(7)

O(8)	0.0917(5)	0.6329(3)	0.0824(4)	0.012(7)
O(9)	0.9262(5)	0.4151(3)	0.4471(4)	0.012(7)

^aU_{eq} is defined as one third of the trace of the orthogonalized U_{ij} tensor.

Table 2.4 Selected bond distances (Å) for $\text{Tl}_2\text{Cu}_2\text{Te}_7\text{O}_{17}$.

Tl(1)-O(1)	2.822(4)	Te(1)-O(1)	1.899(4)	Cu(1)-O(4)	1.925(4)
Tl(1)-O(1)	2.822(4)	Te(1)-O(2)	1.855(4)	Cu(1)-O(4)	1.925(4)
Tl(1)-O(1)	3.059(4)	Te(1)-O(5)	1.910(4)	Cu(1)-O(4)	1.925(4)
Tl(1)-O(1)	3.059(4)			Cu(1)-O(4)	1.925(4)
Tl(1)-O(2)	2.863(4)	Te(2)-O(4)	1.881(4)		
Tl(1)-O(2)	2.863(4)	Te(2)-O(4)	1.881(4)	Cu(2)-O(2)	1.934(4)
Tl(1)-O(3)	3.371(3)	Te(2)-O(5)	2.094(4)	Cu(2)-O(2)	1.934(4)
Tl(1)-O(3)	3.371(2)	Te(2)-O(5)	2.094(4)	Cu(2)-O(2)	1.934(4)
				Cu(2)-O(2)	1.934(4)
		Te(3)-O(1)	2.151(4)	Cu(2)-O(3)	2.210(8)
		Te(3)-O(1)	2.151(4)		
		Te(3)-O(1)	2.151(4)		
		Te(3)-O(1)	2.151(4)		
		Te(3)-O(3)	1.812(8)		

Table 2.5 Selected bond distances (Å) for $\text{Tl}_2\text{Cu}_2\text{Te}_7\text{O}_{18}$.

Tl(1)-O(1)	2.811(4)	Te(2)-O(3)	1.876(4)	Cu(1)-O(1)	1.950(4)
Tl(1)-O(2)	2.852(3)	Te(2)-O(7)	2.096(4)	Cu(1)-O(2)	1.958(4)
Tl(1)-O(3)	2.908(4)	Te(2)-O(9)	1.919(3)	Cu(1)-O(4)	1.956(4)
Tl(1)-O(4)	3.025 (4)	Te(2)-O(9)	2.137(4)	Cu(1)-O(6)	1.950(4)
Tl(1)-O(5)	3.092(4)				
Tl(1)-O(5)	3.346(4)	Te(3)-O(2)	1.864(4)		
Tl(1)-O(6)	3.104(4)	Te(3)-O(3)	2.198(4)		
Tl(1)-O(7)	3.442(4)	Te(3)-O(6)	1.873(4)		
		Te(3)-O(8)	2.129(3)		
Te(1)-O(5)	1.955(3)				
Te(1)-O(5)	1.955(3)	Te(4)-O(1)	1.873(4)		
Te(1)-O(7)	1.939(4)	Te(4)-O(4)	1.869(4)		
Te(1)-O(7)	1.939(4)	Te(4)-O(5)	1.964(4)		
Te(1)-O(8)	1.897(3)				
Te(1)-O(8)	1.897(3)				

Table 2.6 Detailed Bond valence analysis $\text{Tl}_2\text{Cu}_2\text{Te}_7\text{O}_{17}$.

$\text{Tl}_2\text{Cu}_2\text{Te}_7\text{O}_{17}$	O(1)	O(2)	O(3)	O(4)	O(5)	Σ_{cations}
Tl(1)	0.167 ^[x2] 0.104 ^[x2]	0.154 ^[x2]	^[x4] 0.056 ^[x2]			0.962
Te(1)	1.235	1.391			1.199	3.825
Te(2)				1.296 ^[x2]	0.729 ^[x2]	4.050
Te(3)	0.625 ^[x4]		1.562			4.062
Cu(1)				0.514 ^[x4]		2.056
Cu(2)		0.502 ^[x4]	0.238			2.246
Σ_{anions}	2.131	2.047	2.024	1.810	1.928	

Valence sums calculated with the formula: $S_i = \exp[(R_0 - R_i)/B]$, where S_i = valence of bond “ i ”, R_0 is a constant dependent upon the bonded elements, R_i is the bond length of bond i and B equals 0.37 (for Tl^+ , 0.50).

Table 2.7 Detailed Bond valence analysis $\text{Tl}_2\text{Cu}_2\text{Te}_7\text{O}_{18}$.

$\text{Tl}_2\text{Cu}_2\text{Te}_7\text{O}_{18}$	O(1)	O(2)	O(3)	O(4)	O(5)
Tl(1)	0.171	1.157	0.141	0.111	0.097
Te(1)					0.059 0.902 ^[x2]
Te(2)			1.314		
Te(3)		1.357	0.550		
Te(4)	1.325			1.339	1.036
Cu(1)	0.481	0.470		0.473	
Σ_{anions}	1.977	1.984	2.005	1.923	2.094

$\text{Tl}_2\text{Cu}_2\text{Te}_7\text{O}_{18}$	O(6)	O(7)	O(8)	O(9)	Σ_{cations}
Tl(1)	0.059	0.048			0.879
Te(1)		0.942 ^[x2]	1.056 ^[x2]		5.800
Te(2)		0.725		1.170 0.649	3.858
Te(3)	1.325		0.663		3.895
Te(4)					3.700
Cu(1)	0.481				1.905
Σ_{anions}	1.901	1.715	1.719	1.819	

Valence sums calculated with the formula: $S_i = \exp[(R_0 - R_i)/B]$, where S_i = valence of bond “ i ”, R_0 is a constant dependent upon the bonded elements, R_i is the bond length of bond i and B equals 0.37 (for Tl^+ , 0.50).

CHAPTER 3. Syntheses and Crystal Structure of New Polar Potassium Tungsten Selenite: $K_2(WO_3)_3(SeO_3)$

3.1 Abstract

The new polar potassium tungsten selenite, $K_2(WO_3)_3(SeO_3)$ has been synthesized by hydrothermal techniques. The structure of $K_2(WO_3)_3(SeO_3)$ was determined by single crystal X-ray diffraction. The material exhibits a hexagonal tungsten oxide (HTO)-layered structure – class 2, i.e., the WO_6 layers are “capped” on one side by the SeO_3 polyhedra. The K^+ cations are found between the layers. $K_2(WO_3)_3(SeO_3)$ is a non-centrosymmetric and polar space group. Crystal data: $K_2(WO_3)_3(SeO_3)$, trigonal, space group $R3c$ (No. 161), $a = 7.2439(1) \text{ \AA}$, $b = 7.2439(1) \text{ \AA}$, $c = 35.516(7) \text{ \AA}$, $V = 1614.0(5) \text{ \AA}^3$, and $Z = 6$.

3.2 Introduction

Hexagonal tungsten oxide (HTO)-type materials have been studied by many groups. Especially, polar HTO materials are of significant interest due to their functional properties such as second-harmonic generation (SHG), piezoelectricity, ferroelectricity, and pyroelectricity.¹⁻⁴ In addition, their structural diversity is studied since various cations may substitute for W^{6+} as well as A cations^{5,6} ($A = Na^+, K^+, Rb^+, Tl^+$, etc.). The structure of HTO can be described as a hexagonal network of corner-sharing WO_6 octahedra.

We can divide the hexagonal tungsten oxide (HTO)-type materials into class 1 and class 2. For the Class 1, AO_3 lone pair polyhedra ($A = \text{Se}^{4+}$ and Te^{4+}) are directed both “up” and “down”, whereas for the Class 2, AO_3 lone pair polyhedra are directed “up”. In this paper we focus on class 2. With respect to that Class 2 (“capped” on one side) materials have been reported. For example, $\text{A}_2(\text{MoO}_3)_3(\text{SeO}_3)$ ($A = \text{NH}^{4+}$ or Cs^+),⁷ $\text{A}_2(\text{WO}_3)_3(\text{SeO}_3)$ ($A = \text{NH}^{4+}$ or Cs^+)⁸ $\text{A}_2(\text{MoO}_3)_3(\text{PO}_3\text{CH}_3)$ ($A = \text{Rb}^+$, Cs^+ or Tl^+),^{9,10} and $\text{Cs}_2(\text{WO}_3)_3(\text{PO}_3\text{CH}_3)$ ¹¹ by the Jacobson group; $\text{A}_2(\text{MoO}_3)_3(\text{TeO}_3)$ ($A = \text{NH}^{4+}$ or Cs^+)¹² by the Vidyasagar group; $\text{A}_2(\text{MoO}_3)_3(\text{SeO}_3)$ ($A = \text{Rb}^+$ or Tl^+),¹³ $\text{Rb}_2(\text{WO}_3)_3(\text{TeO}_3)$,¹⁴ and $\text{Na}_2(\text{WO}_3)_3(\text{SeO}_3)\cdot 2\text{H}_2\text{O}$ ¹⁵ by the Halasyamani group. In expanding this research toward the synthesis of hexagonal tungsten oxide (HTO)-type materials, we have successfully synthesized potassium d⁰ selenite, $\text{K}_2(\text{WO}_3)_3(\text{SeO}_3)$. The reported material is noncentrosymmetric (NCS) and polar.

In this chapter, synthesis and crystal structures of $\text{K}_2(\text{WO}_3)_3(\text{SeO}_3)$ will be discussed.

3.3 Experimental section

3.3.1 Synthesis

K_2CO_3 (Aldrich, 99%), SeO_2 (Alfa Aesar, 99.4%), and WO_3 (Alfa Aesar, 99.8%) were used as received.

Single crystals of $\text{K}_2(\text{WO}_3)_3(\text{SeO}_3)$, were grown by using hydrothermal techniques. 0.104 g (0.752 mmol) of K_2CO_3 , 0.202 g (1.82 mmol) of SeO_2 , and 0.174 g (0.752 mmol) of WO_3 for $\text{K}_2(\text{WO}_3)_3(\text{SeO}_3)$, were combined with 0.7 mL of distilled water. The solutions were placed in 23 ml Teflon-lined autoclaves that were subsequently closed.

The autoclave was heated to 230 °C, held for 2 days, and cooled slowly to room temperature at a rate of 6 °C/ h. The mother liquor was decanted from the products, and the products were recovered by filtration and washed with distilled water and acetone. Colorless bitrigonal pyramidal-shaped crystals were obtained in ~20 % yield based upon SeO₂.

3.3.2 Characterization

Single Crystal X-ray Diffraction. For K₂(WO₃)₃(SeO₃), a colorless crystal (0.04 × 0.02 × 0.02 mm³) was used for single crystal X-ray diffraction data collection. Data were collected using a Siemens SMART diffractometer equipped with a 1K CCD area detector using graphite-monochromated Mo K α radiation. A hemisphere of data was collected using a narrow-frame method with scan widths of 0.30° in omega and an exposure time of 40 s per frame for K₂(WO₃)₃(SeO₃). The data were integrated using the Siemens SAINT program,¹⁶ with the intensities corrected for Lorentz, polarization, air absorption, and absorption attributable to the variation in the path length through the detector faceplate. Psi-scans were used for the absorption correction on the hemisphere of data. The data were solved by direct methods using SHELXS-97 and refined using SHELXL-97.^{17,18} All of the atoms were refined with anisotropic thermal parameters and converged for $I > 2\sigma(I)$. All calculations were performed using the WinGX-98 crystallographic software package.¹⁹

3.4 Results and discussion

Structure. $\text{K}_2(\text{WO}_3)_3(\text{SeO}_3)$ crystallizes in non-centrosymmetric (NCS) polar trigonal space group $R3c$. The reported material exhibits hexagonal tungsten oxide (HTO)-layered structure, consisting of corner-shared WO_6 octahedra that are “capped” on one side by SeO_3 polyhedra.¹³ The layers are separated by K^+ cations (see Figure 3.1). In connectivity terms, the structure can be described as $[3(\text{WO}_{1/1}\text{O}_{4/2})^- (\text{SeO}_{3/2})^+]^{2-}$, with charge balance maintained by two K^+ cations. The W^{6+} cations are in octahedral coordination environments bonded to six oxygen atoms with one “short” 1.727(5) Å, four “normal” 1.819(7)–2.023(7) Å, and one “long” 2.183 Å W–O bonds.¹⁵ The Se^{4+} cations are in trigonal-pyramidal coordination environments bonded to three oxygen atoms with the same Se–O distance, 1.696(5) Å. Both W^{6+} and Se^{4+} cations are in asymmetric coordination environments attributable to second-order Jahn-Teller (SOJT) effects.²⁰⁻²⁷ The asymmetric coordination environments are caused by W^{6+} cations displaced toward the corner (C_4 -type distortion) and stereoactive lone-pair on the Se^{4+} cations (see Figure 3.2). The K^+ cations are surrounded by six- and nine oxygen atoms with K–O distances ranging from 2.806(6) to 2.974(6) Å. The bond valence calculations^{28,29} for W^{6+} , Se^{4+} , and K^+ resulted in values of 6.173, 4.094, and 0.793–1.302, respectively. Detailed bond valences for $\text{K}_2(\text{WO}_3)_3(\text{SeO}_3)$ are shown in Table 3.4.

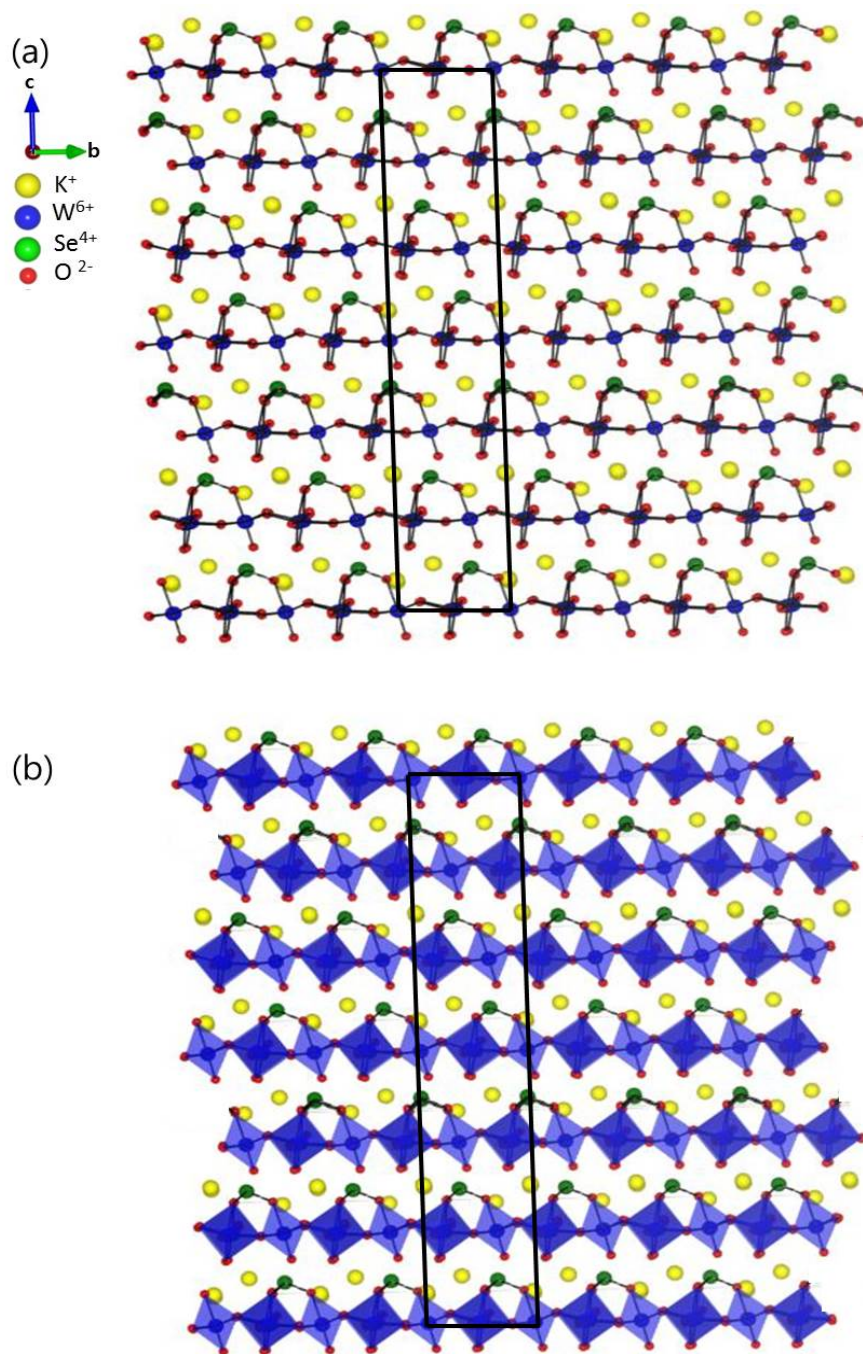


Figure 3.1 Ball-and-stick (a) and polyhedral (b) diagram of $K_2(WO_3)_3(SeO_3)$ in the bc -plane.

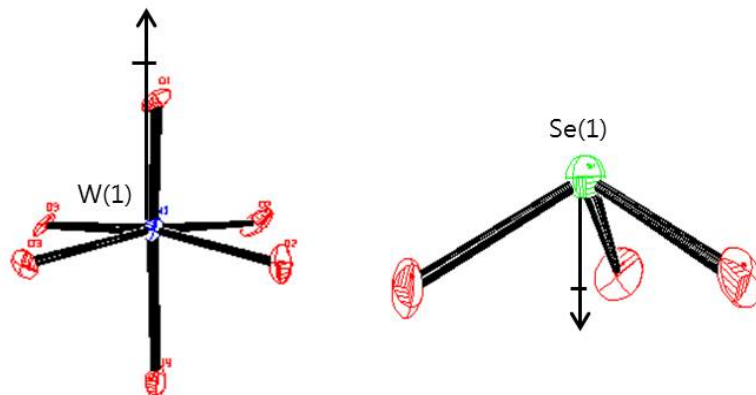


Figure 3.2 ORTEP (50% probability ellipsoids) diagrams for the WO_6 and SeO_3 polyhedra in $\text{K}_2(\text{WO}_3)_3(\text{SeO}_3)$. The arrows represent the approximate directions of the distortion and polarization.

3.5 Conclusion

We have successfully synthesized a new polar potassium tungsten selenite oxide material, $\text{K}_2(\text{WO}_3)_3(\text{SeO}_3)$. Crystals were synthesized by hydrothermal techniques. $\text{K}_2(\text{WO}_3)_3(\text{SeO}_3)$ is non-centrosymmetric (NCS) and crystallizes in the *polar* space group $R3c$. $\text{K}_2(\text{WO}_3)_3(\text{SeO}_3)$ exhibits a class 2 (lone pair polyhedra of SeO_3 groups “capped” on one side) layered hexagonal tungsten oxide (HTO) structure. We are currently in the process of synthesizing a polycrystalline sample by solid state techniques. TGA, IR, UV, SHG, piezoelectricity, pyroelectricity, and ferroelectricity will also be measured.

Table 3.1 Crystallographic data for $K_2(WO_3)_3(SeO_3)$.

formula	$K_2(WO_3)_3(SeO_3)$
fw	900.71
T(K)	293.0(2)
crystal system	Trigonal
space group	$R\ 3c$ (No. 161)
a (Å)	7.2439(1)
b (Å)	7.2439(1)
c (Å)	35.516(7)
α (deg)	90
β (deg)	90
γ (deg)	120
V (Å ³)	1614.0(5)
Z	6
ρ_{calcd} (g/cm ³)	5.560
R (int)	0.0330
GOF (F^2)	1.101
$R(F)^a$	0.0148
$R_w(F_o^2)^b$	0.0359

$$^a R(F) = \frac{\sum ||F_o| - |F_c||}{\sum |F_o|}, \quad ^b R_w(F_o^2) = [\sum w(F_o^2 - F_c^2)^2 / \sum w(F_o^2)^2]^{1/2}$$

Table 3.2 Atomic coordinates and equivalent isotropic displacement parameters (\AA^2) for $\text{K}_2(\text{WO}_3)_3(\text{SeO}_3)$.

	x	y	z	U_{eq}^{a}
K(1)	2/3	1/3	-0.1065(9)	0.030(7)
K(2)	2/3	1/3	0.0905(1)	0.015(5)
Se(1)	1/3	-1/3	0.0839(3)	0.011(2)
W(1)	0.5281(5)	0.0071(7)	0.0048	0.008(9)
O(1)	0.5479(12)	0.0724(8)	-0.0424(2)	0.015(1)
O(2)	0.5805(7)	-0.2130(1)	0.0009(2)	0.013(1)
O(3)	0.7999(1)	0.2182(1)	0.0208(1)	0.011(1)
O(4)	0.0885(8)	-0.4505(1)	0.0637(2)	0.014(1)

^a U_{eq} is defined as one third of the trace of the orthogonalized U_{ij} tensor.

Table 3.3 Selected bond distances (Å) for $\text{K}_2(\text{WO}_3)_3(\text{SeO}_3)$.

K(1)-O(1)	2.806(6)	W(1)-O(1)	1.727(5)	Se(1)-O(4)	1.696(5)
K(1)-O(1)	2.806(6)	W(1)-O(2)	1.819(7)	Se(1)-O(4)	1.696(5)
K(1)-O(1)	2.806(6)	W(1)-O(2)	2.023(7)	Se(1)-O(4)	1.696(5)
K(1)-O(3)	2.974(6)	W(1)-O(3)	1.878(6)		
K(1)-O(3)	2.974(6)	W(1)-O(3)	2.006(7)		
K(1)-O(3)	2.974(6)	W(1)-O(4)	2.183(5)		
K(2)-O(1)	2.816(6)				
K(2)-O(1)	2.816(6)				
K(2)-O(1)	2.816(6)				
K(2)-O(3)	2.925(7)				
K(2)-O(3)	2.925(7)				
K(2)-O(3)	2.925(7)				
K(2)-O(4)	2.812(6)				
K(2)-O(4)	2.812(6)				
K(2)-O(4)	2.812(6)				

Table 3.4 Detailed Bond valence analysis $K_2(WO_3)_3(SeO_3)$.

$K_2(WO_3)_3(SeO_3)$	O(1)	O(2)	O(3)	O(4)	Σ_{cations}
K(1)	0.162 ^[x3]		0.103 ^[x3]		0.793
K(2)	0.157 ^[x3]		0.117 ^[x3]	0.159 ^[x3]	1.302
W(1)	1.671	1.303	1.111	0.550	6.173
Se(1)		0.751	0.786	1.365 ^[x3]	4.094
Σ_{anions}	1.990	2.054	2.117	2.074	

Valence sums calculated with the formula: $S_i = \exp[(R_0 - R_i)/B]$, where S_i = valence of bond "i", R_0 is a constant dependent upon the bonded elements, R_i is the bond length of bond i and B equals 0.37

3.6 References

1. Nye, J. *Physical Properties of Crystals*; Oxford University Press: Oxford, **1957**.
2. Cady, W.G. *Piezoelectricity; an Introduction to the Theory and Applications of Electromechanical Phenomena in Crystals*; Dover: New York, **1964**.
3. Jona, F.; Shirane, G. *Ferroelectric Crystals*; Pergamon Press: Oxford, **1962**.
4. Lang, S. B. *Sourcebook of Pyroelectricity*; Gordon & Breach: London, **1974**.
5. Magneli, A. *Acta Chem. Scand.* **1953**, 7, 315.
6. Lee, K.-S.; D.-K., S.; Whangbo, M. –H. *J. Am. Chem. Soc.* **1997**, 119, 4043
7. Harrison, W. T. A.; Dussack, L. L.; Jacobson, A. J. *J. Inorg. Chem.* **1994**, 33, 6043.
8. Harrison, W. T. A.; Dussack, L. L.; Vogt, T.; Jacobson, A. J. *J. Solid State Chem.* **1995**, 120, 112.
9. Harrison, W. T. A.; Dussack, L. L.; Jacobson, A. J. *J. Inorg. Chem.* **1995**, 34, 4774.
10. Harrison, W. T. A.; Dussack, L. L.; Vogt, T.; Jacobson, A. J. *J. Solid State Chem.* **1998**, 138, 365
11. Harrison, W. T. A.; Dussack, L. L.; Vaughey, J. T.; Vogt, T.; Jacobson, A. J. *J. Mater. Chem.* **1996**, 6, 81
12. Balraj, V.; Vidyasagar, K. *J. Inorg. Chem.* **1998**, 37, 4764.
13. Chang, H. Y.; Kim, S. W.; Halasyamani, P. S. *Chem. Mater.* **2010**, 22, 3241
14. Goodey, J.; Ok, K. M.; Broussard, J.; Hofmann, C.; Escobedo, F. V.; Halasyamani, P. S. *J. Solid State Chem.* **2003**, 175, 3.

15. Nguyen, S. D.; Halasyamani, P. S. *Inorg. Chem.* **2013**, *52*, 2637.
16. SAINT: *A Program for Area Detector Absorption Correction*, Version 4.05; Siemens Analytical X-ray Systems, Inc.: Madison, WI, **1995**.
17. Sheldrick, G. M. *SHELXS-97 - A Program for Crystal Structure Refinement*; University of Goettingen: Goettingen, Germany, **1997**.
18. Sheldrick, G. M. *SHELXL-97 - A Program for Automatic Solution of Crystal Structures*. University of Goettingen: Goettingen, Germany, **1997**.
19. Farrugia, L. J. *J. Appl. Crystallogr.* **1999**, *32*, 837.
20. Opik, U.; Pryce, M. H. L. *Proc. R. Soc. A.* **1957**, *238*, 425.
21. Barder, R. F. W. *Mol. Phys.* **1960**, *3*, 137.
22. Barder, R. F. W. *Can. J. Chem. Phys.* **1962**, *40*, 2140.
23. Pearson, R. G. *J. Am. Chem. Soc.* **1969**, *91*, 4947.
24. Pearson, R. G. *THEOCHEM* **1983**, *12*, 25.
25. Wheeler, R. A.; Whangbo, M. H.; Hughbanks, T.; Hoffmann, R.; Burdett, J. K.; Albright, T. A. *J. Am. Chem. Soc.* **1986**, *108*, 2222.
26. Kunz, M.; Brown, I. D. *J. Solid State Chem.* **1995**, *115*, 395.
27. Goodenough, J. B. *Annu. Rev. Mater. Sci.* **1998**, *28*, 1.
28. Brown, I. D.; Altermatt, D. *Acta Crystallogr., Sect. B* **1985**, *B41*, 244.
29. Brown, I. D. *The Chemical Bond in Inorganic Chemistry*; Oxford University Press: New York, **2012**; Vol. *12*.